DOE-ET-53088-263 IFSR#263

FINITE PRESSURE BALLOONING MODE STABILITY IN TOROIDAL EQUILIBRIA

*X. Llobet,** *H.L. Berk* and *M.N. Rosenbluth*
Institute for Fusion Studies
The University of Texas at Austin
Austin, Texas 78712

* CRPP-EPFL, Lausanne, Switzerland

December 1986

Finite Pressure Ballooning Mode Stability in Toroidal Equilibria

X. LLOBET,[a] H.L. BERK and M.N. ROSENBLUTH

Institute for Fusion Studies

The University of Texas at Austin

Austin, Texas 78712

Abstract

In this paper the effect of finite pressure on the ballooning instability in toroidal MHD equilibria of steep boundary stellarators and tokamaks is examined. Ballooning modes tend to arise near the place where the local shear vanishes and the normal curvature (the curvature component perpendicular to the flux surface, pointing away from the magnetic axis) is negative. It is shown how the pressure gradient determines the position of the shearless points, and demonstrate in detail how this effect explains the existence of second stability in tokamaks. For large aspect ratio circular cross-section tokamaks the second stability condition is found to scale as $\alpha = \text{const}\ S^{1.25}$. Stellarators are inherently more stable, due to the negative vacuum shear which at moderate pressure gradients allows the zero shear point to localize on the inner side of the flux surface. However, at high pressure gradients the Pfirsch-Schlüter current produces a positive mean shear when the total toroidal current on a flux surface is zero. This causes the zero shear point to localize on the outer edge, near the vertical extremes of the flux surface. This effect, together with helical contributions to the helical curvature, allows for ballooning instability to arise. At higher pressure gradients, with zero net toroidal current, an unstable ballooning mode which localizes to within a helical period always arises where the normal curvature is unfavorable.

[a] Present address: CRPP-EPFL, Lausanne, Switzerland

I Introduction

The study of the stability of ballooning modes in tokamaks indicates a critical beta (β_c), for the onset of instability.[1] It is also been established that a "second stability" region with respect to ballooning modes can be reached at yet higher beta.[2,3,4] Ballooning instabilities also appear in stellarators,[5] even though a simplified analysis predicts stability.[6]

Ballooning activity may be relevant in the experiments conducted in tokamaks as the values of beta that have been reached correspond approximately to the predicted critical beta.[7,8] If ballooning modes indeed limit the plasma containment, second stability region allows for a stable plasma configuration at higher beta, provided that a method can be found to avoid or push through the instability region[9,10,11] (and avoid surface modes).

In this paper we attempt to understand in some detail the effect of the pressure gradient on the ballooning instability for tokamaks and stellarators. We use a model of a steep pressure profile equilibrium for both tokamaks and stellarators and examine the stability of a ballooning mode on a flux surface in this steep pressure drop. For the tokamak study we examine a model for a circular cross section and large aspect ratio. For the stellarator we study flux surfaces generated by specific vacuum coils and use analytic techniques to approximate this configuration.

Ballooning instability tends to occur where the local shear vanishes and the local curvature is unfavorable to stability.[2] The local shear is the superposition of the global shear, due to the either force free currents (in tokamaks and current driven stellarators) or external vacuum currents (in stellarators), and the local shear produced by Pfirsch-Schlüter currents, which are proportional to the local pressure gradient. As the pressure gradient increases, the local shear can vanish along the flux tube of a toroidal machine. In tokamaks, where the rotational transform decreases radially outward, the local shear tends to vanish on the outside of the torus, where the normal curvature is unfavorable for stability. This gives rise to ballooning instability. As the pressure gradient increases further the point

of zero shear moves to the top of the torus and eventually the normal curvature becomes too small to induce instability. We will demonstrate through both numerical and analytic treatments the detailed mechanism for this stabilization.

In stellarators,where the rotational transform increases radially outward, the point of zero shear tends to occur on the inside of the torus, where the normal curvature is favorable to stability. At moderate pressure gradients this trait seems to prevent ballooning mode instability if the Mercier coefficient is negative at zero beta[5] (essentially an average min-B system). However, if one assumes there is zero net toroidal current on a flux surface, one can show that, for sufficiently large pressure gradient, the average shear obtained from the Pfirsch-Schlüter currents will change sign. We can show that if we average over helical modulations, the point of zero shear will occur in the region of unfavorable normal curvature. Ballooning instability similar to that found in a tokamak is then possible, but at pressure gradients considerably higher than those usually considered in the tokamak case. At yet higher pressure gradients, the ballooning modes will localize to within a helical ripple, and one can show that there is always instability for arbitrarily high pressure gradients in zero net toroidal current systems.

Despite this conclusion of instability at large pressure gradients, we emphasize that the detailed ballooning calculations confirm the optimistic stability results for stellarators, in that the threshold for instability for average min-B systems first occurs at large pressure gradients, i.e., $(r/B^2)(\partial p/\partial r) \approx 1$, where r is the minor radius and p the pressure.

II Basic Equations

We use magnetic Clebsch coordinates, where the magnetic field is written as $\mathbf{B} = \nabla\psi \times \nabla\beta$. Here ψ labels the flux surface while β labels a field line on the surface, and at fixed toroidal angle β is a poloidal-like angle. It is important to note that on a given surface both $\nabla\psi$ and $\nabla\beta$ can be determined examining only this flux surface. More specifically, they can be computed by following two neighboring field lines belonging to the surface.[5] The vector

$\nabla\beta$ can be decomposed in components parallel and perpendicular to $\nabla\psi$:

$$\nabla\beta = \Lambda_p \nabla\psi + \mathbf{B} \times \nabla\psi / |\nabla\psi|^2. \tag{1}$$

The equation for Λ_p is

$$\mathbf{B} \cdot \nabla\Lambda_p = -|\nabla\psi|^{-4} (\mathbf{B} \times \nabla\psi) \cdot \nabla \times (\mathbf{B} \times \nabla\psi). \tag{2}$$

It can be shown that $d\Lambda_p/ds$ is proportional to the local magnetic shear.[12] The value of Λ_p depends on an arbitrary integration constant which can be viewed as a parameter determining the localization point of the ballooning mode.

The ballooning mode equation, which describes the limit of localizing the excitation to a single field line (e.g. see Ref. 13 for such an interpretation of a ballooning mode) is

$$d/ds \left[\left(|\nabla\beta|^2/B \right) d\xi/ds \right] + (2/B^2)(\partial p/\partial\psi)(\nabla\beta \times \mathbf{b} \cdot \boldsymbol{\kappa})\xi = 0 \tag{3}$$

with $\mathbf{b} = \mathbf{B}/B$, and $\boldsymbol{\kappa} = (\mathbf{b} \cdot \nabla)\mathbf{b}$ is the curvature. This equation follows readily from formal derivation of Ref. 14 in the $\omega \to 0$ limit. One also has the relation $\mathbf{k}_\perp = \Lambda_p \nabla\beta$, with $\mathbf{k}_\perp$ the radial wavenumber. The condition $\Lambda_p = 0$ corresponds to the points where $\mathbf{k}_\perp$ is perpendicular to the flux surface.

Substituting (1) in (3) yields

$$d/ds \left[\left(1 + \Lambda^2 \right) B |\nabla\psi|^{-2} d\xi/ds \right] + (2/B)(\partial p/\partial\psi) |\nabla\psi|^{-1} (\kappa_n - \Lambda\kappa_g)\, \xi = 0 \tag{4}$$

where $\Lambda \equiv \Lambda_p |\nabla\psi|^2/B$, and κ_n and κ_g are the normal and geodesic curvatures: $\boldsymbol{\kappa} = (\kappa_n \nabla\psi + \kappa_g \mathbf{b} \times \nabla\psi)/|\nabla\psi|$. With this definition the normal curvature is negative when $\boldsymbol{\kappa}$ points towards the magnetic axis. With this notation, the energy integral associated with this excitation is

$$W(\xi) = \int ds \left[\left(1 + \Lambda^2 \right) B |\nabla\psi|^{-2} (d\xi/ds)^2 - (2/B)(\partial p/\partial\psi) |\nabla\psi|^{-1} (\kappa_n - \Lambda\kappa_g)\, \xi^2 \right]. \tag{5}$$

We define for later use $\partial p/\partial r = |\nabla\psi| \partial p/\partial\psi$. For circular cross sections r is the poloidal radius.

III Stability Analysis

The ballooning mode equation (4) is complicated by the need to obtain a self-consistent equilibrium to determine the coefficients. However, if we confine ourselves to the case where we consider the field to be given by a zeroth order field (independent of the pressure) plus a modification due to a very steep pressure gradient centered around the flux surface of investigation, we can make substantial progress without solving a global magnetohydrodynamics (MHD) equilibrium code.

The sharp gradient model has been widely used to simplify calculations, and gives reasonable results.[5,15,16] When the plasma pressure is small, but the pressure gradient arbitrary, the most important change in the ballooning equation is in the magnetic shear, which depends on the pressure gradient through the Pfirsch-Schlüter currents. Then $d\Lambda_p/ds$ is given by

$$d\Lambda_p/ds = d\Lambda_p^{(0)}/ds + d\Lambda_p^{(1)}/ds$$

where $d\Lambda_p^{(0)}/ds$ is given by Eq. (2) with vacuum quantities used, and $d\Lambda_p^{(1)}/ds$ is

$$d\Lambda_p^{(1)}/ds = -(j_{||}/B)B|\nabla\psi|^{-2} \tag{6}$$

$$d(j_{||}/B)/ds = 2(\partial p/\partial r)\kappa_g/B^2. \tag{7}$$

The parameter Λ_p then has the following form

$$\Lambda_p(s) = \Lambda_{p0} + \int ds d\Lambda_p^{(0)}/ds + \int ds d\Lambda_p^{(1)}/ds.$$

Λ_{p0} is the integration constant, and can be taken as a label of the ballooning mode. $\Lambda_p(s)$ can be shown to be proportional to the radial wavenumber, and at a given initial point $s = 0$, the choice of Λ_{p0}, which can vary from $-\infty$ to $+\infty$, determines all the possible ballooning modes. In general, the average shear of a field line is not zero, so that $\Lambda_p(s)$ has a non zero secular linear component.

The stability analysis of Eq. (4) can be carried following the method proposed by Newcomb,[17] but using the field line length as the independent variable. If the solution of the

Euler-Lagrange equation (4) has two or more zeros, then $W(\xi)$ can be made negative, and the plasma is unstable. Marginal stability, where $W(\xi) = 0$, is attained when the solution has no zeros and asymptotes to zero faster than $s^{-1/2}$. This solution is the minimizing solution at marginal stability.

To minimize the energy $W(\xi)$ we need to avoid the large positive bending energy, $(1+\Lambda^2)(d\xi/ds)^2$ associated with the shear. This is achieved by allowing ξ to vary primarily where Λ is small. Thus we expect that the minimizing function has significant values mostly in the neighborhood of $\Lambda = 0$ and $d\Lambda/ds = 0$. Instability can then be expected to be favored if in this region $\kappa_n < 0 (\partial p/\partial\psi < 0$ is assumed).

IV Single Point Interaction Model

We assume that it is reasonable to approximate Λ by a power series about the point of zero shear so that $\Lambda = \Lambda_0 + Cs^2/2$. This method is justified if the principal structure of the eigenfunction localizes in the region where the power series expansion is valid. Expanding $j_{||}(s) \approx j_{||}(0) + j'_{||}(0)s$, we have, using (6),

$$\begin{aligned} d\Lambda/ds &\approx \left[d\Lambda_p^{(0)}/ds - j_{||}(s)/|\nabla\psi|^2\right] |\nabla\psi|^2/B \\ &\approx \left[d\Lambda_p^{(0)}/ds - j_{||}(0)/|\nabla\psi|^2\right] |\nabla\psi|^2/B - j'_{||}(0)s/B. \end{aligned}$$

Hence, from (7), we can identify C with $-j'_{||}(0)/B \approx -2(\partial p/\partial r)\kappa_g/B^2$. Thus

$$\Lambda = \Lambda_0 - (\partial p/\partial r)\kappa_g s^2/B^2.$$

With the change of variable $\ell \equiv |(\partial p/\partial r)\kappa_g|^{1/2} s/B$, and assuming that κ_n, κ_g and $|\nabla\psi|$ do not change significantly in the region of interest, we obtain

$$\Lambda = \Lambda_0 + \sigma_g \ell^2$$

$$d/d\ell \left[(1+\Lambda^2) d\xi/d\ell\right] + 2\left(-\kappa_n/|\kappa_g| + \sigma_g\Lambda\right)\xi = 0 \qquad (8)$$

where σ_g is the sign of κ_g. Defining Λ^* as $\Lambda^* \equiv -\sigma_g\Lambda = -\sigma_g\Lambda_0 - \ell^2 \equiv \Lambda_0^* - \ell^2 \equiv \Lambda_0^* - \ell^2$ and $F \equiv -\kappa_n/|\kappa_g|$, the ballooning equation becomes

$$d/d\ell \left[\left(1+\Lambda^*\right) d\xi/d\ell\right] + 2(F - \Lambda^*)\xi = 0 \qquad (9)$$

or, substituting Λ^*,

$$d/d\ell\left\{\left[1+\left(\Lambda_0^*-\ell^2\right)^2\right]d\xi/d\ell\right\}+2\left(F-\Lambda_0^*+\ell^2\right)\xi=0.$$

This equation is readily analyzed and solved. It is important to notice that in this limit the pressure gradient has been scaled away, and that for any solution $\xi(\ell)$ the width in s is inversely proportional to $|\partial p/\partial\psi|^{1/2}$. The only physical parameter remaining in Eq. (9) is the ratio of curvatures at the shearless point, $F=-\kappa_n/|\kappa_g|$; the only sign that matters is the sign of the normal curvature.

We have analyzed this equation numerically by searching for marginal stability, that is, for the solutions without any zeros and tending to zero for large ℓ such that

$$\lim_{\ell\to\infty}\xi(d\xi/d\ell)\ell^4=0.$$

Due to the symmetry of the equation, the eigenmode must be symmetric at marginal stability, and therefore Eq. (9b) is solved with the initial condition $\xi=1$, $d\xi/d\ell=0$ at $\ell=0$. The general asymptotic solutions are of the form $\alpha\ell^{-1}+\beta\ell^{-2}$, and at marginal stability $\alpha=0$ (as on the barely unstable side of marginal stability, $\alpha<0$, guarantees an intersection). Hence, for fixed Λ_0^*, to find the critical positive value F_c we seek an eigenfunction at large ℓ proportional to ℓ^{-2}. If $F<F_c(\Lambda_0^*)$ the configuration is stable, and if $F>F_c(\Lambda_0^*)$ the eigenfunction has two or more zeros, indicating instability. The growth rate, using a simple inertia model, can be estimated by adding to Eq. (9) the term $(1+\Lambda^{*2})\gamma^2\xi$, where γ is the growth rate (in units of $\tau_A^{-1}=\varepsilon v_A(rq)^{-1}$, where ε is the inverse aspect ratio, v_A is the Alfvén velocity, q is the safety factor and r the distance to the magnetic axis). The numerical result for the critical $F_c(\Lambda_0^*)$ is shown as the solid curve of Fig. 1. The value of $F_c(\Lambda_0^*)$ can be approximated by variational methods. For example, using $\xi=(a+b\ell^4)^{-1/2}$, we find $a/b=3\left(1+\Lambda_0^{*2}\right)/5$, and we obtain $F_c^v(\Lambda_0^*)$, an upper bound approximation for $F_c(\Lambda_0^*)$, which is given by $F_c^v=\left\{\left[15\left(1+\Lambda_0^{*2}\right)\right]^{1/2}+3\Lambda_0^*\right\}/8$.This result is plotted as the dashed curve of Fig. 1. For $\Lambda_0^*=0$ we have $F_c(\Lambda_0^*=0)=0.47$ and $F_c^v(\Lambda^*=0)=0.48$; excellent agreement. The variational method works well for $\Lambda_0^*>0$, but fails as $-\Lambda_0^*$ increases.

From the numerical results we observe that the function $F_c(\Lambda_0^*)$ is monotonically decreasing, and for $\Lambda_0^* \to -\infty$ it tends to zero as $(4|\Lambda_0^*|)^{-1}$. Recalling that Λ_0^* is a free parameter (a label for mode localization), it would appear that any shearless point with negative normal curvature can always be the site of a pressure driven ballooning instability as a value of Λ_0^* may always be chosen to make $F_c(\Lambda_0^*) < F$. But this is somewhat misleading. First, the width in ℓ of the eigenfunction tends to grow as $|\Lambda_0^*|^{1/2}$. Thus for a given $\partial p/\partial\psi$, our asymptotic evaluation breaks down at large values of $|\Lambda_0^*|$, when the mode becomes too broad and we have to consider more global aspects of the eigenfunctions along the field line. We will take these considerations into account in the next section where the specific tokamak case is studied. In stellarators, except at extremely high pressure gradients, the period of the helical ripple is shorter than the width of the eigenfunction. This leads to other important considerations in determining the onset of the instability. We will study this effect in the stellarator section.

V Tokamaks

We now apply our analysis to a large aspect ratio circular cross-section tokamak, with the magnetic field given by $\mathbf{B} = B_0(R_0/R)[\hat{\varphi} + b(r)\hat{\theta}]$, where r is the distance to the magnetic axis, R is the distance to the major axis, and θ and φ are the poloidal and toroidal angles, respectively. We introduce the usual shear parameter $S \equiv (r/q)dq/dr = 1 - (r/b)db/dr$, and the dimensionless pressure gradient $\alpha \equiv 2|\partial p/\partial r|r^2/(B_0^2 R_0 b^2)$.

In this case it is more convenient to use θ than s as the independent variable along the field line, due to the axial symmetry; the conversion is given by $bds = rd\theta$. The shear due to the zeroth order field is $d\Lambda_p^{(0)}/d\theta = [S/(1+\varepsilon\cos\theta) - \varepsilon\cos\theta]\, B_0/|\nabla\psi|^2$, with $\varepsilon = r/R_0$ and $|\nabla\psi|^2 = (rB_0)^2$; and the pressure driven shear is $d\Lambda_p^{(1)}/d\theta = -\alpha\cos\theta B_0/|\nabla\psi|^2$, so that the total shear is $d\Lambda_p/d\theta = [S/(1+\varepsilon\cos\theta) - (\alpha+\varepsilon)\cos\theta]\, B_0/|\nabla\psi|^2$. Note that with $S > 0$, which is usually true in tokamaks, the shearless points, determined by $d\Lambda_p/d\theta = 0$, are $\cos\theta_s = [1 - \varepsilon(S+1)/]\, S/\alpha + O(\varepsilon^2)$. As α, the parameter determining the pressure gradient, increases on a flux surface, the shearless point first arises at $\cos\theta_s = 1$, and then

migrates to the top (and to the bottom) as α increases; for $\alpha \gg S$, $F \approx \cos\theta_s \approx s/\alpha$, and $\theta_s \approx \pi/2 - S/\alpha$.

The ballooning mode equation becomes, in the zeroth order in ϵ,

$$d/d\theta \left[(1+\Lambda^2) d\xi/d\theta\right] + \alpha(\cos\theta + \Lambda \sin\theta)\xi = 0 \tag{10}$$

with $\Lambda = A + S\theta - \alpha \sin\theta$, A being the arbitrary constant of integration. In this work we find the constant A more convenient than the common notation $A = -S\theta_k + \alpha \sin\theta_k$.

We have solved Eq. (10) numerically for the marginal second stability point for all choices of the parameter A. In Fig. 2 we show the unstable region in the A-α-plane, for a fixed value of the shear S. Notice the reflection symmetry around $A = 0$, and the periodicity in A, with period $2\pi S$. The use of θ_k instead of A would result in a deformed (and more stretched) version of this figure. The most unstable choices of A are $A = \pm A_{cr} + 2\pi n S$, with A_{cr} indicated in Fig. 2 and n is an integer. The critical value of α for stability at $A = A_{cr}$ we denote as α_{ss}.

In Fig. 3 we have plotted the resulting second stability boundary as a $\log \alpha_{ss}$ vs. $\log\ S$ plot. The empirical second stability criterion that we found approaches the power law

$$\alpha > 4.2 S^{1.25} \tag{11}$$

for the values of S between 2 and 100, and is shown as a solid straight line in Fig. 3. This is a relatively simple criterion which we shall attempt to reproduce analytically. At low values of $S (S < 0.1)$ the second stability criterion agrees with the previously derived estimate[3] $\alpha = 2.13\sqrt{S}$, represented in this Fig. 3 by a dashed line.

Using $y \equiv \xi f^{1/2}$, where $f = 1 + \Lambda^2$, Eq. (10) can be transformed into the equation

$$y'' + y\left\{(\alpha \cos\theta)/f - [(S - \alpha\cos\theta)/f]^2\right\} = 0. \tag{12}$$

In panel (a) of Fig. 4 we have plotted the function Λ for a set of parameters very close to marginal stability. The function $1/f = 1/(1+\Lambda^2)$ is shown in panel (b) of Fig. 4. We observe that for large values of α and S, the function $1/f$ has sharp peaks, of unit value, at

the zeros of Λ, and broader smaller peaks at the negative maxima and positive minima of Λ (only one of these broader peaks is apparent; the other peaks are much smaller). Between these peaks $1/f$ is small ($O(1/S^2)$, $O(1/\alpha^2)$), and the solution to y can be approximated as a straight line, as shown in panel (c), where two numerical solutions of y, corresponding to different values of A (one which is stable, the other which is unstable), are plotted. We observe that the nature of the solution of the differential equation is such that $dy/d\theta$ is constant except where $1/f$ is peaked, where an abrupt change in $dy/d\theta$ occurs. At these points ($\theta = \theta_0$) we can integrate Eq. (12) once assuming that y is constant, to obtain

$$\Delta y' = y \int_{\theta_0-\Delta\theta}^{\theta_0+\Delta\theta} d\theta \left\{-(\alpha\cos\theta)/f + [(S-\alpha\cos\theta)/f]^2\right\}$$

where $\Delta\theta_1 \ll \Delta\theta \ll 1$, and $\Delta\theta_1$ is the width of $1/f$.

We observe that at the zeros of $\Lambda(\Lambda(\theta_z) = 0)$ we can approximate f by $1 + \Lambda'(\theta_z)^2(\theta - \theta_z)^2$, and the change in slope is given by

$$\Delta y'/y \approx (\pi/2)|\Lambda'(\theta_z)|\left[1 - 2\alpha\cos\theta_z/\Lambda'(\theta_z)^2\right] \approx \alpha \tag{13}$$

assuming that $\Lambda'(\theta_z)$ is much larger than $\sqrt{\alpha}$. For the leftmost zero of Λ it can be shown, with the help of Eq. (11), that

$$\Delta y'/y \approx 2\alpha^{0.9}. \tag{14}$$

As this is a large positive jump, it is very stabilizing, independently of the sign of $\Lambda'(\theta_z)$. Hence, if we are to have instability with the initial condition $y(-\infty) = y_{00} = \text{const}$, $y'(-\infty) = 0$, the zero of y has to occur to the left of the first zero of Λ as one moves from left to right. The limiting point is where the zero of y approaches the first zero of Λ.

We now examine the change of slope $\Delta y'/y$ at point M, the first negative maximum of Λ to the left of the first zero of Λ. We see from Fig. 4 that at this point the value of $1/f$ is considerably larger than at the other maxima to the left of M, as previously noted. It will turn out that one can neglect the changes of slope of y at all the negative maxima of Λ except for M.

The first derivative of Λ is $\Lambda' = S - \alpha\cos\theta$, and the second derivative is $\Lambda'' = \alpha\sin\theta$. The shearless points are then given by $\cos\theta_s = S/\alpha$, so that $\alpha\sin\theta_s = \pm(\alpha^2 - S^2)^{1/2} \equiv \pm\alpha_e$.

The plus sign corresponds to a minimum of Λ and the minus sign to a maximum. We choose the negative sign so that θ_s corresponds to a maximum of Λ. Taking θ_s as the origin, we define $\theta = \theta_s + \varphi$ and find that the shear is $\Lambda = \Lambda_0 + \alpha_e(\cos\varphi - 1) + S(\varphi - \sin\varphi)$, with $\Lambda_0 = A + S\theta_s - \alpha\sin\theta_s < 0$. Equation (12) then becomes

$$y'' = y\left\{(-S\cos\varphi - \alpha_e\sin\varphi)/f + [S(1-\cos\varphi) - \alpha_e\sin\varphi]^2/f^2\right\}. \tag{15}$$

In the vicinity of $\varphi = 0$ we can neglect the 1 in f if $\Lambda_0^2 > 1$. We now expand in φ, keeping only the first order contribution of every term, and we obtain

$$\begin{aligned} y'' &= y\left[-S/\Lambda^2 + \alpha_e^2\varphi^2/\Lambda^4\right] \\ \Lambda &= |\Lambda_0| + \alpha_e\varphi^2/2. \end{aligned} \tag{16}$$

If we define $\ell^2 \equiv \alpha_e\varphi^2/2$, Eq. (15) can be written, using $F = S/\alpha_e$,

$$\begin{aligned} d^2y/d\ell^2 &= 2y(-F/\Lambda^2 + 2\ell^2/\Lambda^4) \\ \Lambda &= |\Lambda_0| + \ell^2 \end{aligned} \tag{17}$$

and we recover the parabolic integrated shear approximation used in the previous section.

From Eq. (11) we know that in the parameter range of interest $S \gg 1$ we have $S/\alpha \ll 1$. Now, as we limit ourselves to parameters where the right-hand side is small, Eq. (16) can be solved approximately by iteration, where $y = y_0 + y_1 + \ldots$. Thus, the set of iteration equations takes the form

$$\begin{aligned} y_0'' &= 0 \\ y_1'' &= -y_0\left\{S\cos\varphi/f - [S(1-\cos\varphi) - \alpha_e\sin\varphi]^2/f^2\right\} \\ &\approx -y_0\left[S/\Lambda^2 - \alpha_e^2\varphi^2/\Lambda^4\right] \\ &\quad \text{etc.} \end{aligned}$$

The solution to y_0 is $y_0 = y_{00}$, where we used that to the left of M, $y_0'' = 0$ is a sufficiently accurate approximation to Eq. (15). The next order contribution gives

$$y_1' = -y_{00}\int d\varphi(S/\Lambda^2 - \alpha_e\varphi/\Lambda^4)$$

and we can compute the change in slope integrating over the whole range in φ. We obtain

$$\Delta y_1' = y_{00}\pi(\alpha_e/2)^{1/2}|\Lambda_0|^{-3/2}\left[1/(4|\Lambda_0|) - S/\alpha_e\right]. \tag{18}$$

If there were no constraints on where the intersection occurs, the stability condition would be determined by $\Delta y_1' \geq 0$, that is, $F = S/\alpha_e \leq 1/(4|\Lambda_0|)$. This agrees with the numerical results of the previous section.

It is clear that $\Delta y'/y$ can be of either sign depending on the choice of Λ_0. The most destabilizing choice of $|\Lambda_0|$ is determined by $d(\Delta y')/d|\Lambda_0| = 0$, which gives

$$\Lambda_0 = -5\alpha_e/(12S) \tag{19}$$

and the corresponding change in slope is

$$\Delta y' = -y_{00}\pi(24/25)\sqrt{6/5}S^{2.5}/\alpha^2 = -3.30y_{00}S^{2.5}/\alpha^2. \tag{20}$$

From these equations, and recalling that $S/\alpha \ll 1$ (we can then take $\alpha_e \approx \alpha$), it can be verified that this change in slope is smaller than the change in $\Delta y'/y$ at the first zero of Λ (where $\Delta y'/y = 2\alpha^{0.9}$, cf Eq. (14)), as their ratio is $(S^{2.5}/\alpha^2)/\alpha^{0.9} = (S/\alpha)^{2.5}/\alpha^{0.4} \ll 1/\alpha^{0.4} < 1$. It can also be verified that at S of order one or larger, for Λ_0 values close to Eq. (19), there will be no additional negative maxima of Λ in the interval $\theta_s < \theta < \theta_z$, thereby verifying the consistency of our procedure.

To the left of this maximum, the previous maxima have $|\Lambda_0| = 5\alpha_e/(12S) + 2\pi nS \approx 2\pi nS$, $n = 1, 2, \ldots$, and it is easy to show, using Eqs. (11) and (18), that the change in the slope due to these maxima is smaller than the change due to the last maximum by a factor $0.1S^{15/8} \ll 1$, and that the change in y_0 is also smaller than y_0 by a factor $S^{-15/8}/ \ll 1$.

We now calculate $\theta_z - \theta_s$. We take Λ as

$$\Lambda = \Lambda_0 + S(\theta - \theta_s) - \alpha(\sin\theta - \sin\theta_s)$$

so that $\Lambda(\theta_s) = \Lambda_0$, $\theta_s < 0$. Defining $\theta_z = 3\pi/2 - \eta$, the equation for η is

$$\eta\cos\theta_s - \cos\eta = \Lambda_0/\alpha + (3\pi/2 - \theta_s)\cos\theta_s + \sin\theta_s.$$

Assuming $F \equiv S/\alpha \ll 1$, we have $\sin\theta_s \approx -1 + F^2/2$ and $\theta_s \approx -\pi/2 + F$. Then,

$$\eta F - \cos\eta = \Lambda_0/\alpha + (2\pi - F)F - 1 + F^2/2 = \Lambda_0/\alpha + 2\pi F - 1 + F^2/2.$$

Expanding $\cos\eta$, the solution for η is

$$\eta = -F + 2\pi\left[F/\pi + \Lambda_0/(2\pi^2\alpha)\right]^{1/2}.$$

Hence, the zero of Λ is at a distance $\Delta\varphi$ of the shearless point θ_s given by

$$\Delta\varphi = \theta_z - \theta_s = 2\pi\left\{1 - \left[S/(\alpha\pi) + \Lambda_0/(2\pi^2\alpha)\right]^{1/2}\right\}.$$

The most unstable case is determined by the minimum of the product $\Delta y'\Delta\varphi$, that is, by $d(\Delta y'\Delta\varphi)/d\Lambda_0 = 0$. But the dependence of $\Delta\varphi$ of Λ_0 is sufficiently weak that we can use $d(\Delta y')/d\Lambda_0 = 0$ (as we have already used) to determine the minimizing value of Λ_0. In this case we have seen (Eq. (19)) that Λ_{0cr} is well approximated by $-5\alpha/(12S)$, and we can verify that the term with Λ_0 in $\Delta\varphi$ can be neglected when

$$1 \gg 5\alpha/(24\pi S^2) \approx 0.3S^{-3/4}.$$

Thus we have

$$\Delta\varphi \approx 2\pi\left[1 - \sqrt{S/(\pi\alpha)}\right]. \tag{21}$$

Instability arises if the zero of y occurs before $\varphi = \Delta\varphi$, so that the marginal stability criterion is

$$y_0 + \Delta\varphi\Delta y' = 0$$

which yields

$$\alpha = 4.6S^{1.25}(1 - 0.3S^{-0.125})^{1/2}. \tag{22}$$

In Fig. 3 the numerical criterion given by Eq. (11) and the analytic estimate (22) are compared. The agreement is reasonably close in the range $S > 2$. The departure of the prediction at lower values of S is expected because the analytical method assumes S large. Nonetheless the agreement is still good at $S = 1(\alpha_{\text{estimate}} = 3.8$, Eq. (22); $\alpha_{\text{criterion}} = 4.2$,

Eq. (11), $\alpha_{\text{exact}} = 4.7$). For lower values of S the eigenfunction at marginal stability becomes too wide and encompasses more than one shearless point. Then other analytic methods must be used, such as in Ref. 3.

Thus, we have established the large S behavior of the second stability boundary, extending the results for the low and moderate S regimes: at low S is proportional to $S^{0.5}$ [Ref. 3] while for large S we have shown that scales as $S^{1.25}$ for a large aspect ratio circular tokamak. This result is an improvement over previous estimates,[4] which used that a sufficient condition for second stability is to have the shearless point located in the region of favorable normal curvature. This requirement gives a linear upper bound of the second stability boundary, $\alpha_{ss} < \alpha_{ub} = kS$, with $k \approx 1/[\cos\theta_c]$, where θ_c is the poloidal angle at which the normal curvature changes sign. As in a large aspect ratio circular tokamak $\theta_c \to \pi/2$, $k \to \infty$, this upper bound is not an accurate estimate of the second stability boundary. Recently, L. Chen[18] has reported the scaling $\alpha \propto S^{1.25}$ but with a different proportionality coefficient than ours.

VI Stellarators

We now present our ballooning calculations for stellarators, and in particular we present numerical results for the Proto-Cleo configuration with the steep pressure gradient model described in Ref. 5. The parameters defining the configuration are given in Table I. We have investigated ballooning mode instability in detail on two flux surfaces defined by R at $\varphi = 0$, $\theta = 0$ being 0.435 m and 0.425 m. The Mercier coefficient is negative for both surfaces, and the rotational transforms are found numerically to be 0.457 and 0.243, respectively. The threshold pressure gradients (defined through $\alpha \equiv -2|\partial p/\partial r|R_0/(B_0 t)^2$ with t the rotational transform) for instability are found to be $\alpha(R = 0.435) = 16.7$, $\alpha(R = 0.425) = 157$.

These results indicate that ballooning instability first occurs at relatively high pressure gradients, when compared with tokamak parameters. However, they do occur contrary to Shafranov's speculation that instability will not occur if the Mercier coefficient is negative.

We note that in Ref. 5 it was shown that for the steep pressure profile model the Mercier coefficient will remain negative at arbitrary pressure gradients if it is negative at arbitrarily small pressure gradients.

We interpret the results as follows. Until we reach high pressure gradients the eigenfunction is nearly constant over a helical period, and averages over a single helical period can be considered. Upon averaging one observes that at low and moderate pressure gradients the mean rotational transform increases radially , so that the mean shear, averaged over a poloidal period $\left[d(\Lambda_p^{(0)} + \Lambda_p^{(1)})/ds\right]_{\rm av}$ is negative. Then as the pressure gradient increases, the point of zero shear, i.e., where $d(\Lambda_p^{(0)} + \Lambda_p^{(1)})/ds = 0$ (after a helical average) first occurs on the inside of the torus where the toroidal normal curvature is favorable. With increasing pressure gradient, the point of zero shear moves to the top of torus, where the mean curvature is small. At such pressure gradients two additional effects not considered previously become important. One is the modulation of the normal curvature due to helical effects. The other is that the mean shear can change sign because of the average effects of the Pfirsch-Schlüter current. When this occurs, the point of zero shear (for the zero toroidal current case) will be on the outer side but near the top of the torus. Thus, destabilizing normal curvature from the toroidal fields also drives the ballooning instability at the point of zero shear due to the global effects of the Pfirsch-Schlüter current.

To understand analytically why the mean shear changes sign with pressure we need to integrate Eqs. (6) and (7). With $j_{\|} = 2\lambda B\dfrac{\partial p}{\partial \psi}$, ψ the toroidal flux, and $\mathbf{B}_v = \nabla\Phi_v = \nabla\psi \times \nabla\beta$ ($\mathbf{B}_v$ is the vacuum magnetic field and Φ_v the magnetic potential), eq. (7) can be rewritten as

$$\frac{\partial \lambda}{\partial \Phi_v} = -\frac{1}{2}\frac{\partial}{\partial \beta}\frac{1}{B^2(\Phi_v, \beta, \psi)}.$$

Now, Boozer[19] has shown that

$$\frac{1}{B^2} = \frac{1}{B_N^2}\sum_{n,m}\delta_{n,m}(\psi)\exp\left[i(n - t(\alpha)m)\frac{\Phi_v}{g} + im\beta\right], \tag{23}$$

with $1/B_N^2$ the surface average of $1/B^2$ (which can be written as $\dfrac{1}{B_N^2} = \int_{-\infty}^{\infty}\dfrac{ds}{B}\Big/\int_{-\infty}^{\infty} dsB$) and g the total enclosed poloidal current. The solution for λ, with the condition that the

average value of λ vanishes (which is equivalent to the zero current condition) is

$$\begin{aligned}\lambda &= \frac{g}{2B_N^2}\sum_{n,m}\frac{\delta_{n,m}(\psi)}{\left(\frac{n}{m}-t\right)}\exp\left[i(n-tm)\frac{\Phi_v}{g}-im\beta\right] \\ &\doteq \frac{g}{2B_0^2 t}\sum_m \delta_{0,m}(\psi)\exp\left[-itm\frac{\Phi_v}{g}-im\beta\right] \\ &= \frac{1}{2t}\left(\frac{g}{\langle B\rangle^2}-\frac{g}{B_N^2}\right).\end{aligned}$$

In our approximation we have assumed $t \ll 1$, and we have defined

$$\frac{1}{\langle B^2\rangle} = \frac{1}{B_N^2}+\sum\frac{\delta_{0,m}(\psi)}{B_N^2}\exp\left[-im\left(\frac{t\Phi_v}{g}+\beta\right)\right]$$

as the helical average of g/B^2. In the limit helical perturbations are weak, we also have $g = R_0B_0$, so that

$$\lambda = \frac{R_0B_0}{2t}\left(\frac{1}{\langle B\rangle^2}-\frac{1}{B_N^2}\right).$$

Thus, Eq. (6) becomes

$$d\Lambda_p^{(1)}/ds = (\partial p/\partial\psi)(B_0R_0/t)(1-B^2/B_N^2)/(B|\nabla\psi|^2)$$

where we ignore the helical contribution. The lowest order modulation, using $B \approx B_0(1-\varepsilon\cos\theta)$ and $|\nabla\psi_0| = B_0 r$, is

$$\Lambda^{(1)} = -\alpha\sin\theta$$

(see just after Eq. (4) for the definition of Λ). Thus we recover the tokamak shear modulation (see Eq. (10)). Now one notes that if $|\nabla\psi|^2$ is constant there is no pressure driven contribution to the average shear. To find a change of the average shear the correction to $|\nabla\psi|$ due to the toroidal shift of magnetic surface has to be taken into account. We use $\nabla\psi = \nabla(\psi_0+\psi_1)$, and that ψ_1 is related to the shift Δ by $\Delta\cos\theta = -\psi_1/|\nabla\psi_0|$. From Ref. 20 we have

$$\Delta = -r\varepsilon(4m-1)/[4m(m-1)]$$

and thus

$$\psi_1 = B_0R_0^2(4m-1)/[4m(m-1)]\varepsilon^3\cos\theta.$$

Then

$$|\nabla\psi|^2 = |\nabla(\psi_0+\psi_1)|^2 = |\nabla\psi_0|^2+2\nabla\psi_0\cdot\nabla\psi_1+\ldots = B_0^2r^2\{1+6\varepsilon\cos\theta(4m-1)/[4m(m-1)]\}$$

and the secular component of $\Lambda^{(1)}$ is

$$\Lambda^{(1)} = \alpha 3\varepsilon(4m-1)/[4m(m-1)]\theta \equiv \alpha S_1\theta. \tag{24}$$

The lowest order vacuum shear is readily calculated from Eq. (1) and using $\theta \approx \beta + t\varphi$. This yields

$$\Lambda^{(0)} = -(dt/d\psi)(|\nabla\psi|^2/B)\theta/t = -(d\ell nt/dr)(|\nabla\psi|/B)\theta \approx -(d\ell nt/d\ell nr)\theta.$$

The rotational transform can be expressed, near the axis, as[6]

$$t = \delta_m^2 m^4(m-1)n^{2m-3}/(m!^2 4m)(r/R_0)^{2m-4}.$$

Thus, we obtain

$$\Lambda^{(0)} = -2(m-2)\theta \equiv -S_0\theta$$

and the total integrated shear is

$$\Lambda = (-S_0 + S_1\alpha)\theta - \alpha\sin\theta. \tag{25}$$

This expression predicts the reversal of the shear at

$$\alpha_r = S_0/S_1 = 8m(m-1)(m-2)/[3\varepsilon(4m-1)]$$

which is verified in the numerical code for the Proto-Cleo example.

We now return to the ballooning equation for the tokamak and replace S by $-S_0+S_1\alpha$. We repeat the analysis and write the equation around a point of zero shear. We also need to take into account the helical modulation of the normal curvature, as the absolute value of the normal curvature is small near the zero shear point, which is near the vertical extremes of the flux surface. Thus we add to the toroidal normal curvature a term of the form

$$-R\kappa_n = a\cos p(\varphi-\varphi_0) \tag{26}$$

where $a$is the relative amplitude of the helical modulation (which we have extracted numerically from the actual fields), and p is the ratio of toroidal to helical curvature wavelengths along the field line, and is given by

$$p = (n/t) - m.$$

The phase φ_0 is included because along the field line the relative phase between the helical component and the toroidal shearless point is arbitrary, and we have to consider the worst case for instability.

The reduced ballooning equation for the stellarator is then written as

$$\begin{aligned} y'' &\approx -\alpha_e y \left\{ [F + a\cos\ p(\varphi - \varphi_0)]/\Lambda^2 - \alpha_e \varphi^2/\Lambda^4 \right\} \qquad (27) \\ \Lambda &\approx |\Lambda_0| + \alpha_e \varphi/2 \\ F &= S/\alpha_e = (-S_0 + S_1\alpha_e)/\alpha_e \approx S_1 - S_0/\alpha. \qquad (28) \end{aligned}$$

We solve Eq. (27) as we did in Eq. (15). We write $y = y_0 + y_1 + \ldots$ and we find the equations

$$\begin{aligned} y_0'' &= 0 \qquad (29) \\ y_1'' &\approx -\alpha_e y_0 \left\{ [F + a\ \cos\ p(\varphi - \varphi_0)]/\Lambda^2 - \alpha_e \varphi^2/\Lambda^4 \right\}. \qquad (30) \end{aligned}$$

As before, we take the solution y_0 =constant. Then,

$$\begin{aligned} \Delta y_1' &= -\alpha_e y_0 \int d\varphi \left[F/\Lambda^2 - \alpha_e \varphi^2/ + a\ \cos(p\varphi_0)\cos(p\varphi)/\Lambda^2 \right] \\ &= -y_0 \pi (\alpha_e/2)^{1/2} |\Lambda_0|^{-3/2} \left[F - (4|\Lambda_0|)^{-1} \right. \\ &+ \left. a\ \cos(p\varphi_0) \left(1 + p(2|\Lambda_0|/\alpha_e)^{1/2}\right) \exp\left(-p(2|\Lambda_0|/\alpha_e)^{1/2}\right) \right] \end{aligned}$$

and by demanding an intersection within one toroidal period we obtain the instability condition

$$y_0 + 2\pi \Delta y' < 0$$

which becomes

$$\min[G(|\Lambda_0|)] < 0 \qquad (31)$$

$$G(|\Lambda_0|) \equiv |\Lambda_0|^{3/2} \Big/ \left[(2\alpha_e)^{1/2}\pi^2\right] + (4|\Lambda_0|)^{-1} - F \tag{32}$$

$$-a\left[1 + p(2|\Lambda_0|/\alpha_e)^{1/2}\right] \exp\left[-p(2|\Lambda_0|/\alpha_e)^{1/2}\right] \tag{33}$$

where we have taken the worst phase condition, $\cos(p\varphi_0) = 1$.

Examination of the function G shows that at small α the minimum is positive, indicating the inherent low beta stability of stellarators. As α increases the minimum becomes negative, showing the existence of the ballooning instability. Analytically, we can see that at small the exponential term is very small; neglecting it we recover a tokamak-like criterion: $\min(G) = 0.3\alpha_e^{-1/5} - S/\alpha_e < 0$. More generally when the helical modulation is important we need to solve Eq. (28) numerically.

For the two flux surfaces of the Proto-Cleo that we have investigated we find:

- For $R = 0.435$ m, $S_0 = 2$, $S_1 = 0.13$, $p = 12.3$, $a = 0.7$, the analytic criterion predicts instability at $\alpha = 33$; the numerical code gives $\alpha = 16.7$.
- For $R = 0.425$ m, $S_0 = 2$, $S_0 = 0.094$, $p = 25.8$, $a = 0.5$, the analytic criterion predicts instability at $\alpha = 192$; the numerical codes gives $\alpha = 157$.

We can see that the analytic criterion gives a reasonable estimate of the instability threshold. The relatively bad prediction for the outer line can be partly understood if we consider the behavior of the ratio of the total curvatures. We have modeled the helical contribution in Eq. (26) as a sinusoidal function. However at the outer surface the higher harmonic terms of κ_n are important. Further, our analysis is strictly valid in the limit of large S and at the outer flux surface when $\alpha = 33$, $S = 2.3$, so that our analytic method can have a large error. For the inner flux surface where $\alpha = 192$, $S = 16$, and our method is clearly in the correct regime. Above the instability threshold the eigenfunction will narrow and isolate itself to a helical ripple. In that case the single point interaction analysis of Section IV applies. Instability will always be found as the normal curvature is biased to be destabilizing due to the positive average shear, which is roughly a factor of ε of the toroidal shear modulation, and from the helical contributions to the normal curvature, for

which one can find phases where the contribution is unfavorable. We note that if we allow for toroidal current it is possible to shift the zero shear points to the inside of the cross section, where the normal curvature is favorable.

VII Conclusions

We have examined the ballooning instability in toroidal systems, using a steep pressure gradient model. We can then evaluate the shear produced by the pressure driven Pfirsch-Schlüter currents. By focusing the investigation on the effect of the shearless points that arise when the pressure gradient is increased, we gain some insight in the second stability regime. In tokamaks it can be understood as a consequence of the shifting of these points away from the most unstable regions towards the top of the flux surface, where the destabilizing term is much weaker, and beyond a certain point it is insufficient to drive the instability. We have developed an analytic method that predicts the stability threshold and gives a second stability condition. Our results give a pessimistic outlook to the achieving of second stability since there is a very large unstable region before second stability sets in. However, we have only analyzed a circular cross-section, and considerable improvement in the threshold can be expected with shaping, if the point of zero geodesic curvature can be shifted inward to the region of favorable normal curvature.

In stellarators the case is more complicated. At low pressure gradients the point of zero shear occurs on the inner side of the flux surface, where the normal curvature is stabilizing. However, at large pressure gradients the Pfirsch-Schlüter currents can reverse the sign of the mean shear and one can find first ballooning instability. We further find that the helical modulation of the normal curvature is important in stellarators in establishing the threshold criterion.

We also note that as ballooning instability in stellarators with zero net toroidal current will always arise in the limit of arbitrarily large pressure gradients, it will probably be impossible to generalize the sharp boundary MHD equilibria studied in Ref. 16 to be a lowest order solution of a steep pressure profile MHD equilibria where $\partial p/\partial \psi$ is large. If a

stellarator has up-down symmetry, it may be shown that the marginally stable ballooning mode perturbation can also be made that retains this symmetry. The ballooning mode equation is essentially the same as the equilibrium equation for the line bending produced by the induced parallel currents as the pressure increases. Hence, the instability predicted in linear theory is an indication that ideal MHD equilibrium at a finite width with very large $\partial p/\partial \psi$ profile will not be found. However, it is still possible that the sharp boundary equilibria can be useful to describe sharp profile effects when some non-ideal features, as finite Larmor radius, are included, or if $\partial p/\partial \psi$ is considered bounded as has been treated in this paper.

Acknowledgments

We would like to acknowledge the computational help of Ting Ting Lee. The work was supported by the U.S. Department of Energy contract #DE-FG05-80ET-53088.

References

1. H.P. Furth, J. Killeen, M.N. Rosenbluth, and B. Coppi, in *Plasma Physics and Controlled Nuclear Fusion Research 1965*, (IAEA, Vienna 1966), vol. 1, p. 103.

2. B. Coppi, A. Ferreira, J.W.-K. Mark, and J.J. Ramos, Nucl. Fusion **19**, 715 (1979).

3. D. Lortz, and J.Nühremberg, Phys. Lett. **68A**, 49 (1978).

4. J.M. Greene, and M.S. Chance, Nucl. Fusion **21**, 453 (1981).

5. H.L. Berk, M.N. Rosenbluth, and J.L. Shohet, Phys. Fluids **26**, 2616 (1983).

6. V.D. Shafranov, Phys. Fluids **26**, 357 (1983).

7. M.S. Chance, R.L. Dewar, E.A. Frieman, A.H. Glasser, J.M. Greene, R. C. Grimm, S.C. Jardin, J.L. Johnson, J. Manickam, M. Okabayashi, and A.M. Todd, in *Plasma Physics and Controlled Nuclear Fusion Research* (Proc. 7th Int. Conf., Innsbruck, 1978), (IAEA, Vienna, 1979), vol. 1, p. 677; R.C. Grimm, R.L. Dewar, and J. Manickam, J. Comput. Phys. **49**, 194 (1983).

8. K.M. McGuire, Proc. Int. Conf. Plasma Physics, Proceedings Invited Papers, M.Q. Tran and R.J. Verbeek, Eds., Lausanne (1984) Vol. I, p. 123; C.K. Chu, A. Deniz, G.E. Georgiou, R.A. Gross, A.A. Grossman, A. Holland, R. Izzo, C. Kostek, F.M. Levinton, H.C. Lui, M. Machida, T.C. Marshall, R.L. Merlino, D. Oepts, G.A. Navratil, and P.G. Weber, Nucl. Fusion **25**, 1109 (1985).

9. M.N. Rosenbluth, S.T. Tsai, J.W. Van Dam, and M.G. Engquist, Phys. Rev. Lett. **51**, 1967 (1983).

10. A. Sykes, and M.F. Turner, in *Controlled Fusion and Plasma Physics* (Proc. 9th Europ. Conf., Oxford, 1979), (Culham Lab., Abingdon, U.K., 1979) EP22.

11. M.S. Chance, S.C. Jardin, and T.H. Stix, Phys. Rev. Lett. **51**, 1963 (1983).

12. J.M. Greene and J.L. Johnson, Plasma Phys. **10**, 729 (1968).

13. K.V. Roberts and J.B. Taylor, Phys. Fluids **8**, 315 (1965).

14. R.L. Dewar and A.H. Glasser, Phys. Fluids **26**, 3038 (1983).

15. J.P. Freidberg, Rev. Mod. Phys. **54**, 801 (1982).

16. H.L. Berk, J.P. Freidberg, X. Llobet, P.J. Morrison, and J.A. Tataronis, Phys. Fluids **29**, 3281 (1986).

17. W. Newcomb, Ann. Phys. **10**, 232 (1960).

18. Liu Chen and M.S. Chance, Bull. Am. Phys. Soc. **31** 9, 1603 (1986).

19. A.H. Boozer, Phys. Fluids **24**, 1999 (1981).

20. A.I. Morozov, and L.S. Solov'ev, in *Reviews of Plasma Physics*, (Consultants Bureau, New York, 1965), vol. 2, p. 1.

Characteristic		
Major radius	$R_0(m)$	0.400
Minor radius	$a(m)$	0.093
Number of field periods	n	7
Winding multipolarity	m	3
Winding law		$\phi = (m/n)\theta$
Number of helices		2
θ_{helix} and $\phi = 0$		0
		60°
Helical currents	(MA)	± 0.020
Toroidal field current	(MA)	0.600

Table I. Parameters determining magnetic fields in Proto-Cleo. Coils are wound around a surface of revolution generated by rotating a circle of radius a whose center is a distance R_0 from the axis. The toroidal angle is ϕ and the poloidal angle is θ.

Figure Captions

Figure 1. The solid curve shows the critical value of the parameter F in the single interaction model, $F_c(\Lambda_0)$. The dashed line is the variational upper bound $F_c^v(\Lambda_0)$, and the dotted line is the limit $-1/(4\Lambda_0)$ of $F_c(\Lambda_0)$ at large negative values of Λ_0.

Figure 2. Ballooning instability domain in the A-plane, at $S = 10.0$.

Figure 3. Second stability boundary as a function $\log\alpha$ vs. $\log\ S$. The dots denote the numerical solution, and the solid straight line is a linear fit at large values of S. The dashed line is the prediction at low S given in Ref. 3. The crosses represent the criterion obtained in this paper.

Figure 4. Several computed quantities of Eq. (16). Panel (a) shows the integrated shear function Λ for a case very close to second stability: $S = 10.0$, $\alpha = 60.93$, $A = 15.10$. In panel (b) the function $1/f$ is plotted. Panel (c) shows the graphs of the solution y of the Schrödinger equation (Eq. (4)) for two different values of the parameter A: the top graph is for $A = 15.11$ (stable), the bottom graph is for $A = 15.09$ (unstable).

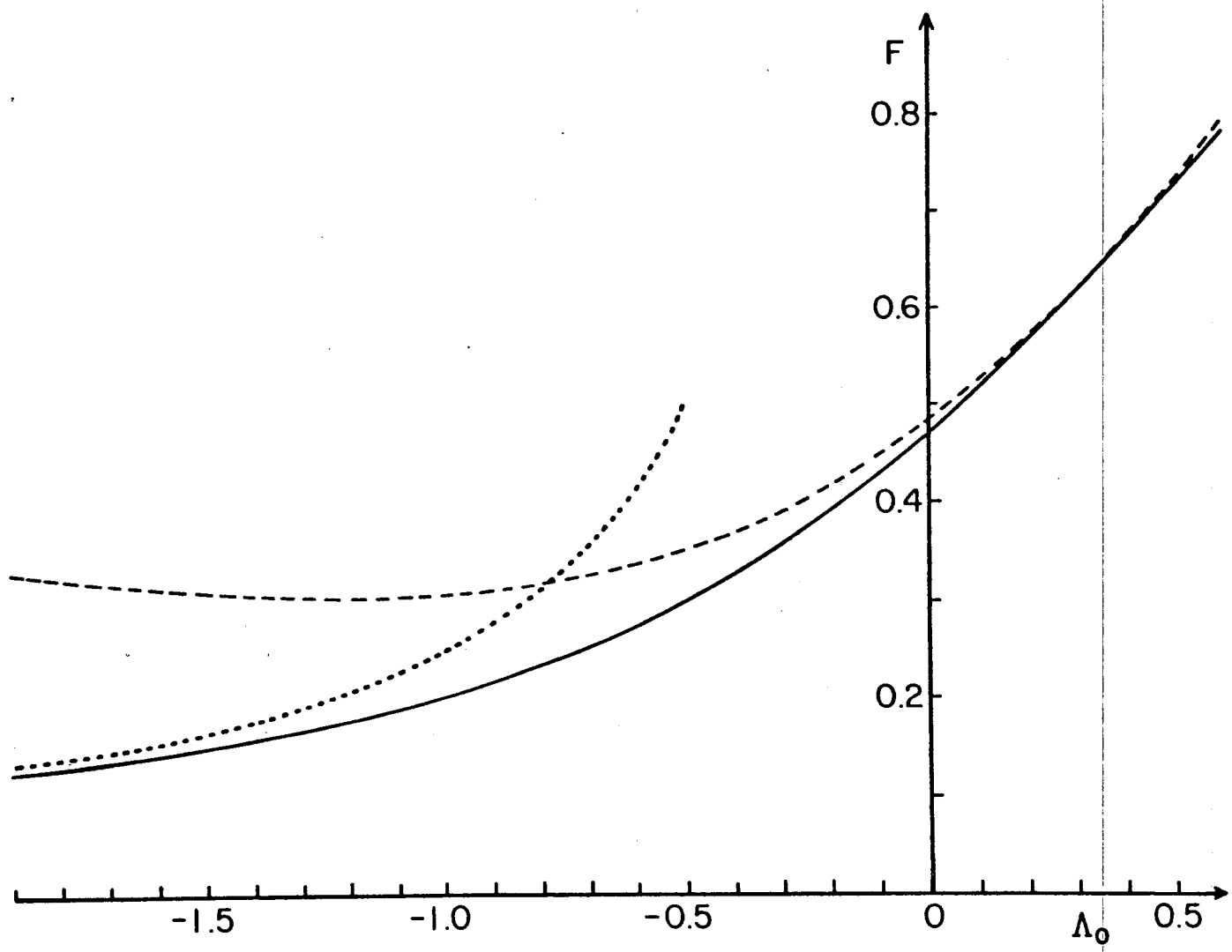

Fig. 1

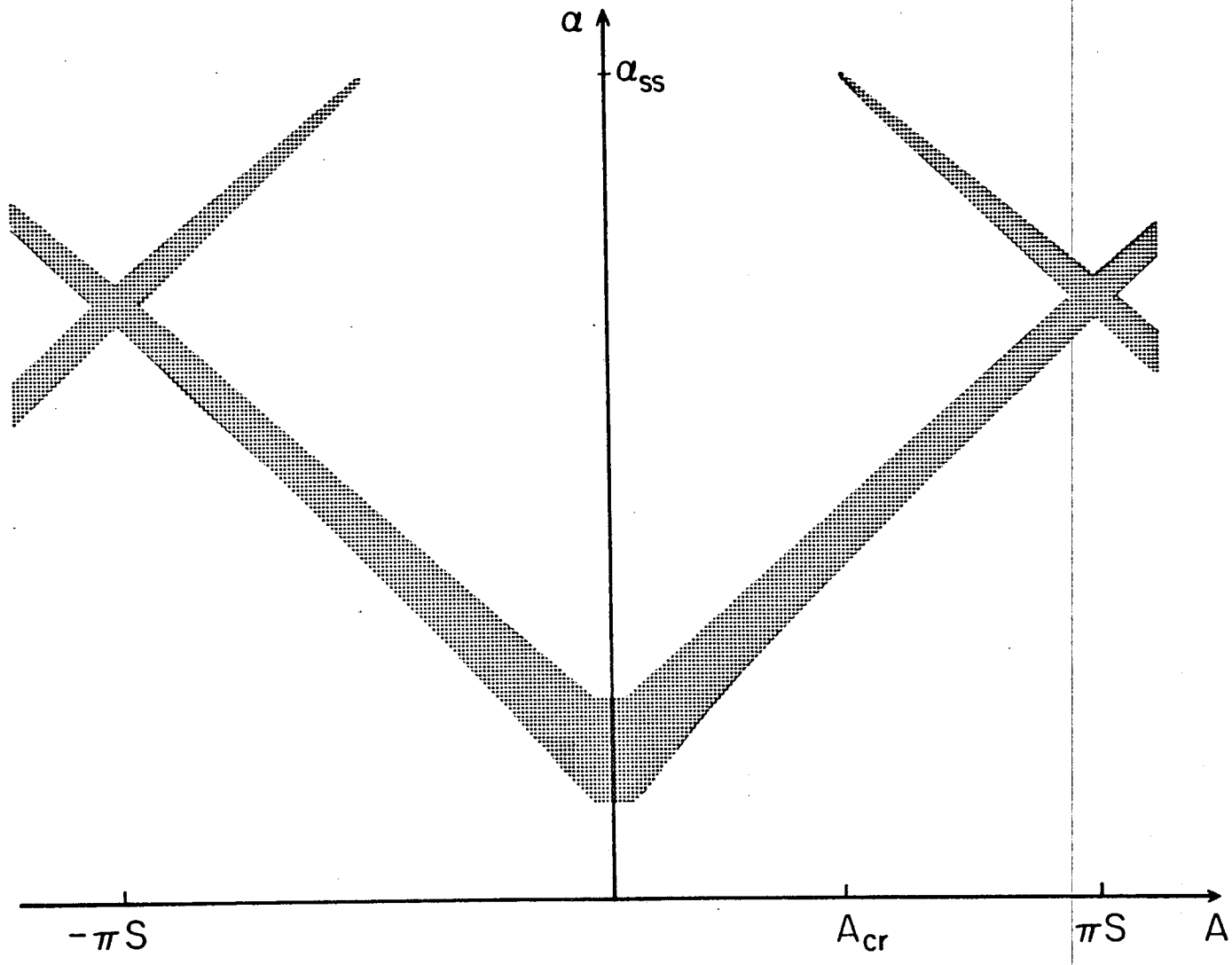

Fig. 2

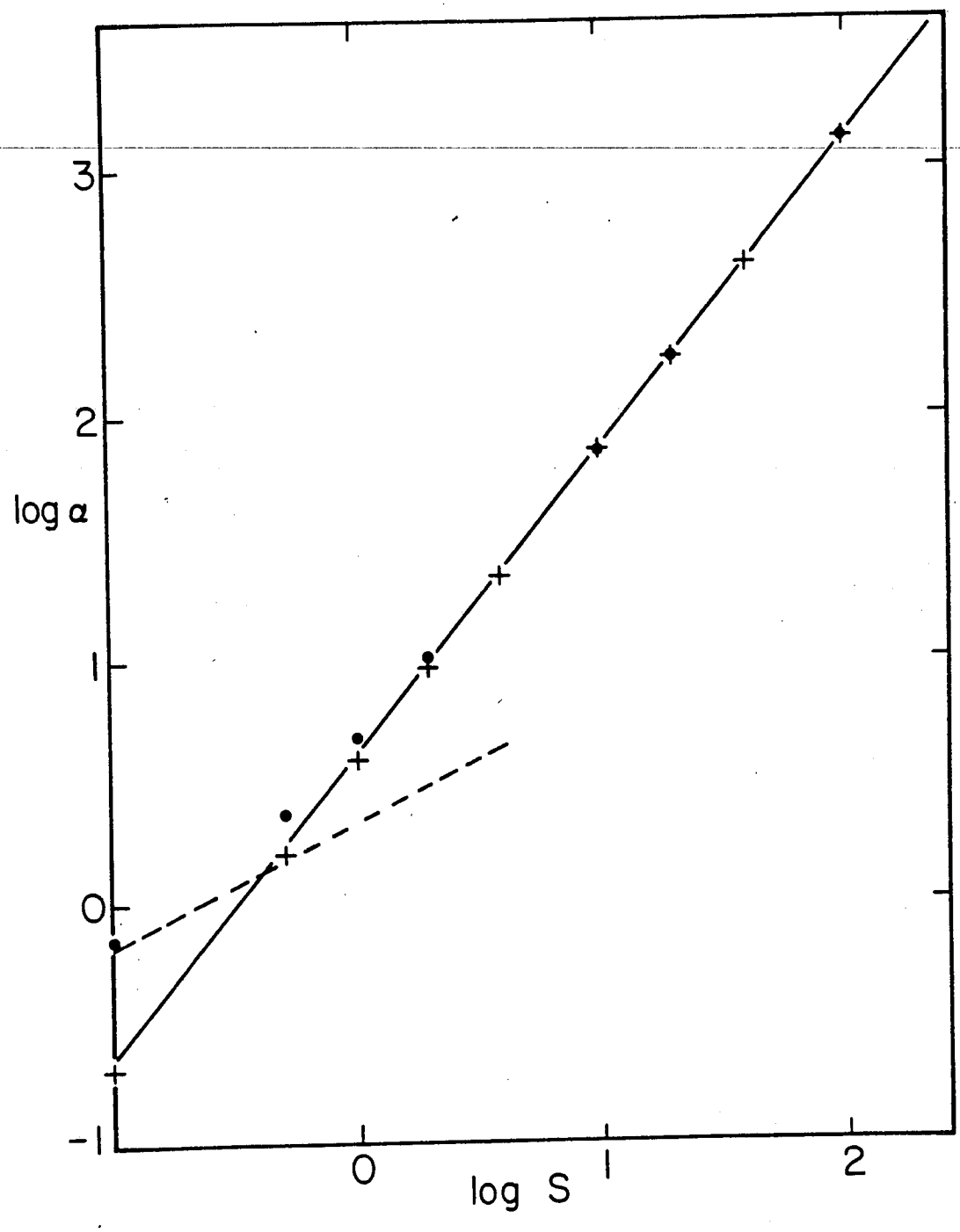

Fig. 3

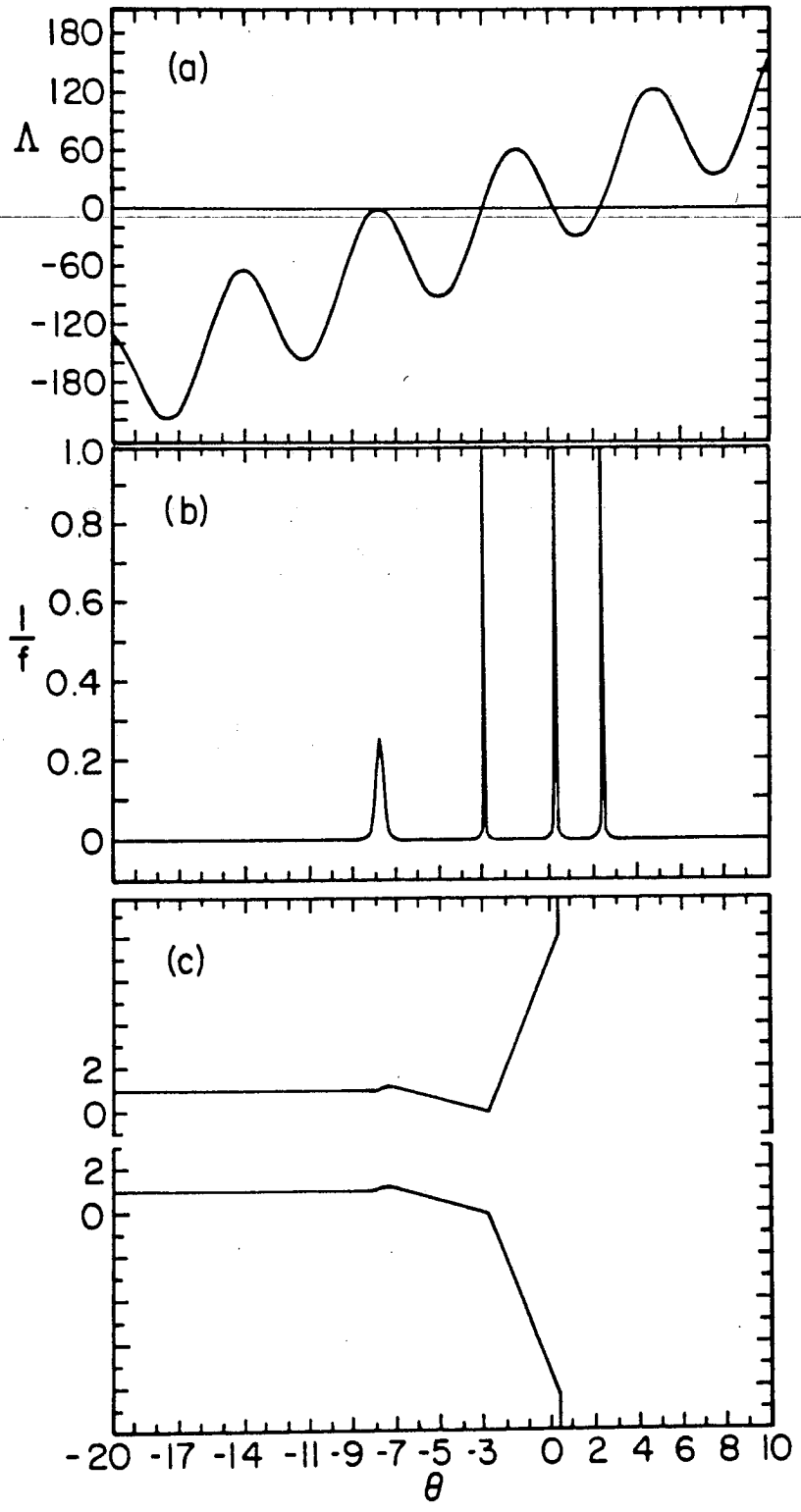
(a)
Λ
180
120
60
0
-60
-120
-180
(b)
1/f
1.0
0.8
0.6
0.4
0.2
0
(c)
2
0
2
0
-20 -17 -14 -11 -9 -7 -5 -3 0 2 4 6 8 10
θ

Fig. 4

Finite Pressure Ballooning Mode Stability in Toroidal Equilibria

X. LLOBET,[a] H.L. BERK and M.N. ROSENBLUTH

Institute for Fusion Studies

The University of Texas at Austin

Austin, Texas 78712

Abstract

In this paper the effect of finite pressure on the ballooning instability in toroidal MHD equilibria of steep boundary stellarators and tokamaks is examined. Ballooning modes tend to arise near the place where the local shear vanishes and the normal curvature (the curvature component perpendicular to the flux surface, pointing away from the magnetic axis) is negative. It is shown how the pressure gradient determines the position of the shearless points, and demonstrate in detail how this effect explains the existence of second stability in tokamaks. For large aspect ratio circular cross-section tokamaks the second stability condition is found to scale as $\alpha = \text{const}\ S^{1.25}$. Stellarators are inherently more stable, due to the negative vacuum shear which at moderate pressure gradients allows the zero shear point to localize on the inner side of the flux surface. However, at high pressure gradients the Pfirsch-Schlüter current produces a positive mean shear when the total toroidal current on a flux surface is zero. This causes the zero shear point to localize on the outer edge, near the vertical extremes of the flux surface. This effect, together with helical contributions to the helical curvature, allows for ballooning instability to arise. At higher pressure gradients, with zero net toroidal current, an unstable ballooning mode which localizes to within a helical period always arises where the normal curvature is unfavorable.

[a] Present address: CRPP-EPFL, Lausanne, Switzerland

I Introduction

The study of the stability of ballooning modes in tokamaks indicates a critical beta (β_c), for the onset of instability.[1] It is also been established that a "second stability" region with respect to ballooning modes can be reached at yet higher beta.[2,3,4] Ballooning instabilities also appear in stellarators,[5] even though a simplified analysis predicts stability.[6]

Ballooning activity may be relevant in the experiments conducted in tokamaks as the values of beta that have been reached correspond approximately to the predicted critical beta.[7,8] If ballooning modes indeed limit the plasma containment, second stability region allows for a stable plasma configuration at higher beta, provided that a method can be found to avoid or push through the instability region[9,10,11] (and avoid surface modes).

In this paper we attempt to understand in some detail the effect of the pressure gradient on the ballooning instability for tokamaks and stellarators. We use a model of a steep pressure profile equilibrium for both tokamaks and stellarators and examine the stability of a ballooning mode on a flux surface in this steep pressure drop. For the tokamak study we examine a model for a circular cross section and large aspect ratio. For the stellarator we study flux surfaces generated by specific vacuum coils and use analytic techniques to approximate this configuration.

Ballooning instability tends to occur where the local shear vanishes and the local curvature is unfavorable to stability.[2] The local shear is the superposition of the global shear, due to the either force free currents (in tokamaks and current driven stellarators) or external vacuum currents (in stellarators), and the local shear produced by Pfirsch-Schlüter currents, which are proportional to the local pressure gradient. As the pressure gradient increases, the local shear can vanish along the flux tube of a toroidal machine. In tokamaks, where the rotational transform decreases radially outward, the local shear tends to vanish on the outside of the torus, where the normal curvature is unfavorable for stability. This gives rise to ballooning instability. As the pressure gradient increases further the point

of zero shear moves to the top of the torus and eventually the normal curvature becomes too small to induce instability. We will demonstrate through both numerical and analytic treatments the detailed mechanism for this stabilization.

In stellarators,where the rotational transform increases radially outward, the point of zero shear tends to occur on the inside of the torus, where the normal curvature is favorable to stability. At moderate pressure gradients this trait seems to prevent ballooning mode instability if the Mercier coefficient is negative at zero beta[5] (essentially an average min-B system). However, if one assumes there is zero net toroidal current on a flux surface, one can show that, for sufficiently large pressure gradient, the average shear obtained from the Pfirsch-Schlüter currents will change sign. We can show that if we average over helical modulations, the point of zero shear will occur in the region of unfavorable normal curvature. Ballooning instability similar to that found in a tokamak is then possible, but at pressure gradients considerably higher than those usually considered in the tokamak case. At yet higher pressure gradients, the ballooning modes will localize to within a helical ripple, and one can show that there is always instability for arbitrarily high pressure gradients in zero net toroidal current systems.

Despite this conclusion of instability at large pressure gradients, we emphasize that the detailed ballooning calculations confirm the optimistic stability results for stellarators, in that the threshold for instability for average min-B systems first occurs at large pressure gradients, i.e., $(r/B^2)(\partial p/\partial r) \approx 1$, where r is the minor radius and p the pressure.

II Basic Equations

We use magnetic Clebsch coordinates, where the magnetic field is written as $\mathbf{B} = \nabla\psi \times \nabla\beta$. Here ψ labels the flux surface while β labels a field line on the surface, and at fixed toroidal angle β is a poloidal-like angle. It is important to note that on a given surface both $\nabla\psi$ and $\nabla\beta$ can be determined examining only this flux surface. More specifically, they can be computed by following two neighboring field lines belonging to the surface.[5] The vector

$\nabla\beta$ can be decomposed in components parallel and perpendicular to $\nabla\psi$:

$$\nabla\beta = \Lambda_p \nabla\psi + \mathbf{B} \times \nabla\psi / |\nabla\psi|^2. \tag{1}$$

The equation for Λ_p is

$$\mathbf{B} \cdot \nabla\Lambda_p = -|\nabla\psi|^{-4} (\mathbf{B} \times \nabla\psi) \cdot \nabla \times (\mathbf{B} \times \nabla\psi). \tag{2}$$

It can be shown that $d\Lambda_p/ds$ is proportional to the local magnetic shear.[12] The value of Λ_p depends on an arbitrary integration constant which can be viewed as a parameter determining the localization point of the ballooning mode.

The ballooning mode equation, which describes the limit of localizing the excitation to a single field line (e.g. see Ref. 13 for such an interpretation of a ballooning mode) is

$$d/ds \left[\left(|\nabla\beta|^2/B \right) d\xi/ds \right] + (2/B^2)(\partial p/\partial\psi)(\nabla\beta \times \mathbf{b} \cdot \boldsymbol{\kappa})\xi = 0 \tag{3}$$

with $\mathbf{b} = \mathbf{B}/B$, and $\boldsymbol{\kappa} = (\mathbf{b} \cdot \nabla)\mathbf{b}$ is the curvature. This equation follows readily from formal derivation of Ref. 14 in the $\omega \to 0$ limit. One also has the relation $\mathbf{k}_\perp = \Lambda_p \nabla\beta$, with $\mathbf{k}_\perp$ the radial wavenumber. The condition $\Lambda_p = 0$ corresponds to the points where $\mathbf{k}_\perp$ is perpendicular to the flux surface.

Substituting (1) in (3) yields

$$d/ds \left[\left(1 + \Lambda^2 \right) B |\nabla\psi|^{-2} d\xi/ds \right] + (2/B)(\partial p/\partial\psi) |\nabla\psi|^{-1} (\kappa_n - \Lambda\kappa_g)\, \xi = 0 \tag{4}$$

where $\Lambda \equiv \Lambda_p |\nabla\psi|^2/B$, and κ_n and κ_g are the normal and geodesic curvatures: $\boldsymbol{\kappa} = (\kappa_n \nabla\psi + \kappa_g \mathbf{b} \times \nabla\psi) / |\nabla\psi|$. With this definition the normal curvature is negative when $\boldsymbol{\kappa}$ points towards the magnetic axis. With this notation, the energy integral associated with this excitation is

$$W(\xi) = \int ds \left[\left(1 + \Lambda^2 \right) B |\nabla\psi|^{-2} (d\xi/ds)^2 - (2/B)(\partial p/\partial\psi) |\nabla\psi|^{-1} (\kappa_n - \Lambda\kappa_g)\, \xi^2 \right]. \tag{5}$$

We define for later use $\partial p/\partial r = |\nabla\psi| \partial p/\partial\psi$. For circular cross sections r is the poloidal radius.

III Stability Analysis

The ballooning mode equation (4) is complicated by the need to obtain a self-consistent equilibrium to determine the coefficients. However, if we confine ourselves to the case where we consider the field to be given by a zeroth order field (independent of the pressure) plus a modification due to a very steep pressure gradient centered around the flux surface of investigation, we can make substantial progress without solving a global magnetohydrodynamics (MHD) equilibrium code.

The sharp gradient model has been widely used to simplify calculations, and gives reasonable results.[5,15,16] When the plasma pressure is small, but the pressure gradient arbitrary, the most important change in the ballooning equation is in the magnetic shear, which depends on the pressure gradient through the Pfirsch-Schlüter currents. Then $d\Lambda_p/ds$ is given by

$$d\Lambda_p/ds = d\Lambda_p^{(0)}/ds + d\Lambda_p^{(1)}/ds$$

where $d\Lambda_p^{(0)}/ds$ is given by Eq. (2) with vacuum quantities used, and $d\Lambda_p^{(1)}/ds$ is

$$d\Lambda_p^{(1)}/ds = -(j_{||}/B)B|\nabla\psi|^{-2} \tag{6}$$

$$d(j_{||}/B)/ds = 2(\partial p/\partial r)\kappa_g/B^2. \tag{7}$$

The parameter Λ_p then has the following form

$$\Lambda_p(s) = \Lambda_{p0} + \int ds d\Lambda_p^{(0)}/ds + \int ds d\Lambda_p^{(1)}/ds.$$

Λ_{p0} is the integration constant, and can be taken as a label of the ballooning mode. $\Lambda_p(s)$ can be shown to be proportional to the radial wavenumber, and at a given initial point $s = 0$, the choice of Λ_{p0}, which can vary from $-\infty$ to $+\infty$, determines all the possible ballooning modes. In general, the average shear of a field line is not zero, so that $\Lambda_p(s)$ has a non zero secular linear component.

The stability analysis of Eq. (4) can be carried following the method proposed by Newcomb,[17] but using the field line length as the independent variable. If the solution of the

Euler-Lagrange equation (4) has two or more zeros, then $W(\xi)$ can be made negative, and the plasma is unstable. Marginal stability, where $W(\xi) = 0$, is attained when the solution has no zeros and asymptotes to zero faster than $s^{-1/2}$. This solution is the minimizing solution at marginal stability.

To minimize the energy $W(\xi)$ we need to avoid the large positive bending energy, $(1+\Lambda^2)(d\xi/ds)^2$ associated with the shear. This is achieved by allowing ξ to vary primarily where Λ is small. Thus we expect that the minimizing function has significant values mostly in the neighborhood of $\Lambda = 0$ and $d\Lambda/ds = 0$. Instability can then be expected to be favored if in this region $\kappa_n < 0 (\partial p/\partial\psi < 0$ is assumed).

IV Single Point Interaction Model

We assume that it is reasonable to approximate Λ by a power series about the point of zero shear so that $\Lambda = \Lambda_0 + Cs^2/2$. This method is justified if the principal structure of the eigenfunction localizes in the region where the power series expansion is valid. Expanding $j_{||}(s) \approx j_{||}(0) + j'_{||}(0)s$, we have, using (6),

$$\begin{aligned} d\Lambda/ds &\approx \left[d\Lambda_p^{(0)}/ds - j_{||}(s)/|\nabla\psi|^2\right] |\nabla\psi|^2/B \\ &\approx \left[d\Lambda_p^{(0)}/ds - j_{||}(0)/|\nabla\psi|^2\right] |\nabla\psi|^2/B - j'_{||}(0)s/B. \end{aligned}$$

Hence, from (7), we can identify C with $-j'_{||}(0)/B \approx -2(\partial p/\partial r)\kappa_g/B^2$. Thus

$$\Lambda = \Lambda_0 - (\partial p/\partial r)\kappa_g s^2/B^2.$$

With the change of variable $\ell \equiv |(\partial p/\partial r)\kappa_g|^{1/2}\, s/B$, and assuming that κ_n, κ_g and $|\nabla\psi|$ do not change significantly in the region of interest, we obtain

$$\Lambda = \Lambda_0 + \sigma_g \ell^2$$

$$d/d\ell \left[(1+\Lambda^2) d\xi/d\ell\right] + 2\left(-\kappa_n/|\kappa_g| + \sigma_g\Lambda\right)\xi = 0 \qquad (8)$$

where σ_g is the sign of κ_g. Defining Λ^* as $\Lambda^* \equiv -\sigma_g\Lambda = -\sigma_g\Lambda_0 - \ell^2 \equiv \Lambda_0^* - \ell^2 \equiv \Lambda_0^* - \ell^2$ and $F \equiv -\kappa_n/|\kappa_g|$, the ballooning equation becomes

$$d/d\ell \left[\left(1+\Lambda^*\right) d\xi/d\ell\right] + 2(F - \Lambda^*)\xi = 0 \qquad (9)$$

or, substituting Λ^*,

$$d/d\ell\left\{\left[1+\left(\Lambda_0^*-\ell^2\right)^2\right]d\xi/d\ell\right\}+2\left(F-\Lambda_0^*+\ell^2\right)\xi=0.$$

This equation is readily analyzed and solved. It is important to notice that in this limit the pressure gradient has been scaled away, and that for any solution $\xi(\ell)$ the width in s is inversely proportional to $|\partial p/\partial\psi|^{1/2}$. The only physical parameter remaining in Eq. (9) is the ratio of curvatures at the shearless point, $F=-\kappa_n/|\kappa_g|$; the only sign that matters is the sign of the normal curvature.

We have analyzed this equation numerically by searching for marginal stability, that is, for the solutions without any zeros and tending to zero for large ℓ such that

$$\lim_{\ell\to\infty}\xi(d\xi/d\ell)\ell^4=0.$$

Due to the symmetry of the equation, the eigenmode must be symmetric at marginal stability, and therefore Eq. (9b) is solved with the initial condition $\xi=1$, $d\xi/d\ell=0$ at $\ell=0$. The general asymptotic solutions are of the form $\alpha\ell^{-1}+\beta\ell^{-2}$, and at marginal stability $\alpha=0$ (as on the barely unstable side of marginal stability, $\alpha<0$, guarantees an intersection). Hence, for fixed Λ_0^*, to find the critical positive value F_c we seek an eigenfunction at large ℓ proportional to ℓ^{-2}. If $F<F_c(\Lambda_0^*)$ the configuration is stable, and if $F>F_c(\Lambda_0^*)$ the eigenfunction has two or more zeros, indicating instability. The growth rate, using a simple inertia model, can be estimated by adding to Eq. (9) the term $(1+\Lambda^{*2})\gamma^2\xi$, where γ is the growth rate (in units of $\tau_A^{-1}=\varepsilon v_A(rq)^{-1}$, where ε is the inverse aspect ratio, v_A is the Alfvén velocity, q is the safety factor and r the distance to the magnetic axis). The numerical result for the critical $F_c(\Lambda_0^*)$ is shown as the solid curve of Fig. 1. The value of $F_c(\Lambda_0^*)$ can be approximated by variational methods. For example, using $\xi=(a+b\ell^4)^{-1/2}$, we find $a/b=3\left(1+\Lambda_0^{*2}\right)/5$, and we obtain $F_c^v(\Lambda_0^*)$, an upper bound approximation for $F_c(\Lambda_0^*)$, which is given by $F_c^v=\left\{\left[15\left(1+\Lambda_0^{*2}\right)\right]^{1/2}+3\Lambda_0^*\right\}/8$.This result is plotted as the dashed curve of Fig. 1. For $\Lambda_0^*=0$ we have $F_c(\Lambda_0^*=0)=0.47$ and $F_c^v(\Lambda^*=0)=0.48$; excellent agreement. The variational method works well for $\Lambda_0^*>0$, but fails as $-\Lambda_0^*$ increases.

From the numerical results we observe that the function $F_c(\Lambda_0^*)$ is monotonically decreasing, and for $\Lambda_0^* \to -\infty$ it tends to zero as $(4|\Lambda_0^*|)^{-1}$. Recalling that Λ_0^* is a free parameter (a label for mode localization), it would appear that any shearless point with negative normal curvature can always be the site of a pressure driven ballooning instability as a value of Λ_0^* may always be chosen to make $F_c(\Lambda_0^*) < F$. But this is somewhat misleading. First, the width in ℓ of the eigenfunction tends to grow as $|\Lambda_0^*|^{1/2}$. Thus for a given $\partial p/\partial\psi$, our asymptotic evaluation breaks down at large values of $|\Lambda_0^*|$, when the mode becomes too broad and we have to consider more global aspects of the eigenfunctions along the field line. We will take these considerations into account in the next section where the specific tokamak case is studied. In stellarators, except at extremely high pressure gradients, the period of the helical ripple is shorter than the width of the eigenfunction. This leads to other important considerations in determining the onset of the instability. We will study this effect in the stellarator section.

V Tokamaks

We now apply our analysis to a large aspect ratio circular cross-section tokamak, with the magnetic field given by $\mathbf{B} = B_0(R_0/R)[\hat{\varphi} + b(r)\hat{\theta}]$, where r is the distance to the magnetic axis, R is the distance to the major axis, and θ and φ are the poloidal and toroidal angles, respectively. We introduce the usual shear parameter $S \equiv (r/q)dq/dr = 1 - (r/b)db/dr$, and the dimensionless pressure gradient $\alpha \equiv 2|\partial p/\partial r|r^2/(B_0^2 R_0 b^2)$.

In this case it is more convenient to use θ than s as the independent variable along the field line, due to the axial symmetry; the conversion is given by $bds = rd\theta$. The shear due to the zeroth order field is $d\Lambda_p^{(0)}/d\theta = [S/(1+\varepsilon\cos\theta) - \varepsilon\cos\theta]\, B_0/|\nabla\psi|^2$, with $\varepsilon = r/R_0$ and $|\nabla\psi|^2 = (rB_0)^2$; and the pressure driven shear is $d\Lambda_p^{(1)}/d\theta = -\alpha\cos\theta B_0/|\nabla\psi|^2$, so that the total shear is $d\Lambda_p/d\theta = [S/(1+\varepsilon\cos\theta) - (\alpha+\varepsilon)\cos\theta]\, B_0/|\nabla\psi|^2$. Note that with $S > 0$, which is usually true in tokamaks, the shearless points, determined by $d\Lambda_p/d\theta = 0$, are $\cos\theta_s = [1 - \varepsilon(S+1)/]\, S/\alpha + O(\varepsilon^2)$. As α, the parameter determining the pressure gradient, increases on a flux surface, the shearless point first arises at $\cos\theta_s = 1$, and then

migrates to the top (and to the bottom) as α increases; for $\alpha \gg S$, $F \approx \cos\theta_s \approx s/\alpha$, and $\theta_s \approx \pi/2 - S/\alpha$.

The ballooning mode equation becomes, in the zeroth order in ε,

$$d/d\theta \left[(1+\Lambda^2) d\xi/d\theta\right] + \alpha(\cos\theta + \Lambda \sin\theta)\xi = 0 \tag{10}$$

with $\Lambda = A + S\theta - \alpha \sin\theta$, A being the arbitrary constant of integration. In this work we find the constant A more convenient than the common notation $A = -S\theta_k + \alpha \sin\theta_k$.

We have solved Eq. (10) numerically for the marginal second stability point for all choices of the parameter A. In Fig. 2 we show the unstable region in the A-α-plane, for a fixed value of the shear S. Notice the reflection symmetry around $A = 0$, and the periodicity in A, with period $2\pi S$. The use of θ_k instead of A would result in a deformed (and more stretched) version of this figure. The most unstable choices of A are $A = \pm A_{cr} + 2\pi n S$, with A_{cr} indicated in Fig. 2 and n is an integer. The critical value of α for stability at $A = A_{cr}$ we denote as α_{ss}.

In Fig. 3 we have plotted the resulting second stability boundary as a $\log \alpha_{ss}$ vs. $\log S$ plot. The empirical second stability criterion that we found approaches the power law

$$\alpha > 4.2 S^{1.25} \tag{11}$$

for the values of S between 2 and 100, and is shown as a solid straight line in Fig. 3. This is a relatively simple criterion which we shall attempt to reproduce analytically. At low values of $S (S < 0.1)$ the second stability criterion agrees with the previously derived estimate[3] $\alpha = 2.13\sqrt{S}$, represented in this Fig. 3 by a dashed line.

Using $y \equiv \xi f^{1/2}$, where $f = 1 + \Lambda^2$, Eq. (10) can be transformed into the equation

$$y'' + y\left\{(\alpha \cos\theta)/f - [(S - \alpha\cos\theta)/f]^2\right\} = 0. \tag{12}$$

In panel (a) of Fig. 4 we have plotted the function Λ for a set of parameters very close to marginal stability. The function $1/f = 1/(1+\Lambda^2)$ is shown in panel (b) of Fig. 4. We observe that for large values of α and S, the function $1/f$ has sharp peaks, of unit value, at

the zeros of Λ, and broader smaller peaks at the negative maxima and positive minima of Λ (only one of these broader peaks is apparent; the other peaks are much smaller). Between these peaks $1/f$ is small ($O(1/S^2)$, $O(1/\alpha^2)$), and the solution to y can be approximated as a straight line, as shown in panel (c), where two numerical solutions of y, corresponding to different values of A (one which is stable, the other which is unstable), are plotted. We observe that the nature of the solution of the differential equation is such that $dy/d\theta$ is constant except where $1/f$ is peaked, where an abrupt change in $dy/d\theta$ occurs. At these points ($\theta = \theta_0$) we can integrate Eq. (12) once assuming that y is constant, to obtain

$$\Delta y' = y \int_{\theta_0-\Delta\theta}^{\theta_0+\Delta\theta} d\theta \left\{-(\alpha\cos\theta)/f + [(S-\alpha\cos\theta)/f]^2\right\}$$

where $\Delta\theta_1 \ll \Delta\theta \ll 1$, and $\Delta\theta_1$ is the width of $1/f$.

We observe that at the zeros of $\Lambda(\Lambda(\theta_z) = 0)$ we can approximate f by $1 + \Lambda'(\theta_z)^2(\theta - \theta_z)^2$, and the change in slope is given by

$$\Delta y'/y \approx (\pi/2)|\Lambda'(\theta_z)|\left[1 - 2\alpha\cos\theta_z/\Lambda'(\theta_z)^2\right] \approx \alpha \tag{13}$$

assuming that $\Lambda'(\theta_z)$ is much larger than $\sqrt{\alpha}$. For the leftmost zero of Λ it can be shown, with the help of Eq. (11), that

$$\Delta y'/y \approx 2\alpha^{0.9}. \tag{14}$$

As this is a large positive jump, it is very stabilizing, independently of the sign of $\Lambda'(\theta_z)$. Hence, if we are to have instability with the initial condition $y(-\infty) = y_{00} = \text{const}$, $y'(-\infty) = 0$, the zero of y has to occur to the left of the first zero of Λ as one moves from left to right. The limiting point is where the zero of y approaches the first zero of Λ.

We now examine the change of slope $\Delta y'/y$ at point M, the first negative maximum of Λ to the left of the first zero of Λ. We see from Fig. 4 that at this point the value of $1/f$ is considerably larger than at the other maxima to the left of M, as previously noted. It will turn out that one can neglect the changes of slope of y at all the negative maxima of Λ except for M.

The first derivative of Λ is $\Lambda' = S - \alpha\cos\theta$, and the second derivative is $\Lambda'' = \alpha\sin\theta$. The shearless points are then given by $\cos\theta_s = S/\alpha$, so that $\alpha\sin\theta_s = \pm(\alpha^2 - S^2)^{1/2} \equiv \pm\alpha_e$.

The plus sign corresponds to a minimum of Λ and the minus sign to a maximum. We choose the negative sign so that θ_s corresponds to a maximum of Λ. Taking θ_s as the origin, we define $\theta = \theta_s + \varphi$ and find that the shear is $\Lambda = \Lambda_0 + \alpha_e(\cos\varphi - 1) + S(\varphi - \sin\varphi)$, with $\Lambda_0 = A + S\theta_s - \alpha\sin\theta_s < 0$. Equation (12) then becomes

$$y'' = y\left\{\left(-S\cos\varphi - \alpha_e\sin\varphi\right)/f + \left[S(1-\cos\varphi) - \alpha_e\sin\varphi\right]^2/f^2\right\}. \tag{15}$$

In the vicinity of $\varphi = 0$ we can neglect the 1 in f if $\Lambda_0^2 > 1$. We now expand in φ, keeping only the first order contribution of every term, and we obtain

$$\begin{aligned} y'' &= y\left[-S/\Lambda^2 + \alpha_e^2\varphi^2/\Lambda^4\right] \\ \Lambda &= |\Lambda_0| + \alpha_e\varphi^2/2. \end{aligned} \tag{16}$$

If we define $\ell^2 \equiv \alpha_e\varphi^2/2$, Eq. (15) can be written, using $F = S/\alpha_e$,

$$\begin{aligned} d^2y/d\ell^2 &= 2y(-F/\Lambda^2 + 2\ell^2/\Lambda^4) \\ \Lambda &= |\Lambda_0| + \ell^2 \end{aligned} \tag{17}$$

and we recover the parabolic integrated shear approximation used in the previous section.

From Eq. (11) we know that in the parameter range of interest $S \gg 1$ we have $S/\alpha \ll 1$. Now, as we limit ourselves to parameters where the right-hand side is small, Eq. (16) can be solved approximately by iteration, where $y = y_0 + y_1 + \ldots$. Thus, the set of iteration equations takes the form

$$\begin{aligned} y_0'' &= 0 \\ y_1'' &= -y_0\left\{S\cos\varphi/f - \left[S(1-\cos\varphi) - \alpha_e\sin\varphi\right]^2/f^2\right\} \\ &\approx -y_0\left[S/\Lambda^2 - \alpha_e^2\varphi^2/\Lambda^4\right] \\ &\quad \text{etc.} \end{aligned}$$

The solution to y_0 is $y_0 = y_{00}$, where we used that to the left of M, $y_0'' = 0$ is a sufficiently accurate approximation to Eq. (15). The next order contribution gives

$$y_1' = -y_{00}\int d\varphi(S/\Lambda^2 - \alpha_e\varphi/\Lambda^4)$$

and we can compute the change in slope integrating over the whole range in φ. We obtain

$$\Delta y_1' = y_{00}\pi(\alpha_e/2)^{1/2}|\Lambda_0|^{-3/2}\left[1/(4|\Lambda_0|) - S/\alpha_e\right]. \tag{18}$$

If there were no constraints on where the intersection occurs, the stability condition would be determined by $\Delta y_1' \geq 0$, that is, $F = S/\alpha_e \leq 1/(4|\Lambda_0|)$. This agrees with the numerical results of the previous section.

It is clear that $\Delta y'/y$ can be of either sign depending on the choice of Λ_0. The most destabilizing choice of $|\Lambda_0|$ is determined by $d(\Delta y')/d|\Lambda_0| = 0$, which gives

$$\Lambda_0 = -5\alpha_e/(12S) \tag{19}$$

and the corresponding change in slope is

$$\Delta y' = -y_{00}\pi(24/25)\sqrt{6/5}S^{2.5}/\alpha^2 = -3.30y_{00}S^{2.5}/\alpha^2. \tag{20}$$

From these equations, and recalling that $S/\alpha \ll 1$ (we can then take $\alpha_e \approx \alpha$), it can be verified that this change in slope is smaller than the change in $\Delta y'/y$ at the first zero of Λ (where $\Delta y'/y = 2\alpha^{0.9}$, cf Eq. (14)), as their ratio is $(S^{2.5}/\alpha^2)/\alpha^{0.9} = (S/\alpha)^{2.5}/\alpha^{0.4} \ll 1/\alpha^{0.4} < 1$. It can also be verified that at S of order one or larger, for Λ_0 values close to Eq. (19), there will be no additional negative maxima of Λ in the interval $\theta_s < \theta < \theta_z$, thereby verifying the consistency of our procedure.

To the left of this maximum, the previous maxima have $|\Lambda_0| = 5\alpha_e/(12S) + 2\pi nS \approx 2\pi nS$, $n = 1, 2, \ldots$, and it is easy to show, using Eqs. (11) and (18), that the change in the slope due to these maxima is smaller than the change due to the last maximum by a factor $0.1S^{15/8} \ll 1$, and that the change in y_0 is also smaller than y_0 by a factor $S^{-15/8}/ \ll 1$.

We now calculate $\theta_z - \theta_s$. We take Λ as

$$\Lambda = \Lambda_0 + S(\theta - \theta_s) - \alpha(\sin\theta - \sin\theta_s)$$

so that $\Lambda(\theta_s) = \Lambda_0$, $\theta_s < 0$. Defining $\theta_z = 3\pi/2 - \eta$, the equation for η is

$$\eta\cos\theta_s - \cos\eta = \Lambda_0/\alpha + (3\pi/2 - \theta_s)\cos\theta_s + \sin\theta_s.$$

Assuming $F \equiv S/\alpha \ll 1$, we have $\sin\theta_s \approx -1 + F^2/2$ and $\theta_s \approx -\pi/2 + F$. Then,

$$\eta F - \cos\eta = \Lambda_0/\alpha + (2\pi - F)F - 1 + F^2/2 = \Lambda_0/\alpha + 2\pi F - 1 + F^2/2.$$

Expanding $\cos\eta$, the solution for η is

$$\eta = -F + 2\pi\left[F/\pi + \Lambda_0/(2\pi^2\alpha)\right]^{1/2}.$$

Hence, the zero of Λ is at a distance $\Delta\varphi$ of the shearless point θ_s given by

$$\Delta\varphi = \theta_z - \theta_s = 2\pi\left\{1 - \left[S/(\alpha\pi) + \Lambda_0/(2\pi^2\alpha)\right]^{1/2}\right\}.$$

The most unstable case is determined by the minimum of the product $\Delta y'\Delta\varphi$, that is, by $d(\Delta y'\Delta\varphi)/d\Lambda_0 = 0$. But the dependence of $\Delta\varphi$ of Λ_0 is sufficiently weak that we can use $d(\Delta y')/d\Lambda_0 = 0$ (as we have already used) to determine the minimizing value of Λ_0. In this case we have seen (Eq. (19)) that $\Lambda_{0\mathrm{cr}}$ is well approximated by $-5\alpha/(12S)$, and we can verify that the term with Λ_0 in $\Delta\varphi$ can be neglected when

$$1 \gg 5\alpha/(24\pi S^2) \approx 0.3S^{-3/4}.$$

Thus we have

$$\Delta\varphi \approx 2\pi\left[1 - \sqrt{S/(\pi\alpha)}\right]. \tag{21}$$

Instability arises if the zero of y occurs before $\varphi = \Delta\varphi$, so that the marginal stability criterion is

$$y_0 + \Delta\varphi\Delta y' = 0$$

which yields

$$\alpha = 4.6S^{1.25}(1 - 0.3S^{-0.125})^{1/2}. \tag{22}$$

In Fig. 3 the numerical criterion given by Eq. (11) and the analytic estimate (22) are compared. The agreement is reasonably close in the range $S > 2$. The departure of the prediction at lower values of S is expected because the analytical method assumes S large. Nonetheless the agreement is still good at $S = 1(\alpha_{\mathrm{estimate}} = 3.8$, Eq. (22); $\alpha_{\mathrm{criterion}} = 4.2$,

Eq. (11), $\alpha_{\text{exact}} = 4.7$). For lower values of S the eigenfunction at marginal stability becomes too wide and encompasses more than one shearless point. Then other analytic methods must be used, such as in Ref. 3.

Thus, we have established the large S behavior of the second stability boundary, extending the results for the low and moderate S regimes: at low S is proportional to $S^{0.5}$ [Ref. 3] while for large S we have shown that scales as $S^{1.25}$ for a large aspect ratio circular tokamak. This result is an improvement over previous estimates,[4] which used that a sufficient condition for second stability is to have the shearless point located in the region of favorable normal curvature. This requirement gives a linear upper bound of the second stability boundary, $\alpha_{ss} < \alpha_{ub} = kS$, with $k \approx 1/[\cos\theta_c]$, where θ_c is the poloidal angle at which the normal curvature changes sign. As in a large aspect ratio circular tokamak $\theta_c \to \pi/2$, $k \to \infty$, this upper bound is not an accurate estimate of the second stability boundary. Recently, L. Chen[18] has reported the scaling $\alpha \propto S^{1.25}$ but with a different proportionality coefficient than ours.

VI Stellarators

We now present our ballooning calculations for stellarators, and in particular we present numerical results for the Proto-Cleo configuration with the steep pressure gradient model described in Ref. 5. The parameters defining the configuration are given in Table I. We have investigated ballooning mode instability in detail on two flux surfaces defined by R at $\varphi = 0$, $\theta = 0$ being 0.435 m and 0.425 m. The Mercier coefficient is negative for both surfaces, and the rotational transforms are found numerically to be 0.457 and 0.243, respectively. The threshold pressure gradients (defined through $\alpha \equiv -2|\partial p/\partial r|R_0/(B_0 t)^2$ with t the rotational transform) for instability are found to be $\alpha(R = 0.435) = 16.7$, $\alpha(R = 0.425) = 157$.

These results indicate that ballooning instability first occurs at relatively high pressure gradients, when compared with tokamak parameters. However, they do occur contrary to Shafranov's speculation that instability will not occur if the Mercier coefficient is negative.

We note that in Ref. 5 it was shown that for the steep pressure profile model the Mercier coefficient will remain negative at arbitrary pressure gradients if it is negative at arbitrarily small pressure gradients.

We interpret the results as follows. Until we reach high pressure gradients the eigenfunction is nearly constant over a helical period, and averages over a single helical period can be considered. Upon averaging one observes that at low and moderate pressure gradients the mean rotational transform increases radially , so that the mean shear, averaged over a poloidal period $\left[d(\Lambda_p^{(0)} + \Lambda_p^{(1)})/ds\right]_{\rm av}$ is negative. Then as the pressure gradient increases, the point of zero shear, i.e., where $d(\Lambda_p^{(0)} + \Lambda_p^{(1)})/ds = 0$ (after a helical average) first occurs on the inside of the torus where the toroidal normal curvature is favorable. With increasing pressure gradient, the point of zero shear moves to the top of torus, where the mean curvature is small. At such pressure gradients two additional effects not considered previously become important. One is the modulation of the normal curvature due to helical effects. The other is that the mean shear can change sign because of the average effects of the Pfirsch-Schlüter current. When this occurs, the point of zero shear (for the zero toroidal current case) will be on the outer side but near the top of the torus. Thus, destabilizing normal curvature from the toroidal fields also drives the ballooning instability at the point of zero shear due to the global effects of the Pfirsch-Schlüter current.

To understand analytically why the mean shear changes sign with pressure we need to integrate Eqs. (6) and (7). With $j_{||} = 2\lambda B\dfrac{\partial p}{\partial \psi}$, ψ the toroidal flux, and $\mathbf{B}_v = \nabla\Phi_v = \nabla\psi \times \nabla\beta$ ($\mathbf{B}_v$ is the vacuum magnetic field and Φ_v the magnetic potential), eq. (7) can be rewritten as

$$\frac{\partial \lambda}{\partial \Phi_v} = -\frac{1}{2}\frac{\partial}{\partial \beta}\frac{1}{B^2(\Phi_v, \beta, \psi)}.$$

Now, Boozer[19] has shown that

$$\frac{1}{B^2} = \frac{1}{B_N^2}\sum_{n,m}\delta_{n,m}(\psi)\exp\left[i(n - t(\alpha)m)\frac{\Phi_v}{g} + im\beta\right], \tag{23}$$

with $1/B_N^2$ the surface average of $1/B^2$ (which can be written as $\dfrac{1}{B_N^2} = \displaystyle\int_{-\infty}^{\infty}\frac{ds}{B}\Big/\int_{-\infty}^{\infty} dsB$) and g the total enclosed poloidal current. The solution for λ, with the condition that the

average value of λ vanishes (which is equivalent to the zero current condition) is

$$\begin{aligned}\lambda &= \frac{g}{2B_N^2}\sum_{n,m}\frac{\delta_{n,m}(\psi)}{\left(\frac{n}{m}-t\right)}\exp\left[i(n-tm)\frac{\Phi_v}{g}-im\beta\right] \\ &\doteqdot \frac{g}{2B_0^2 t}\sum_m \delta_{0,m}(\psi)\exp\left[-itm\frac{\Phi_v}{g}-im\beta\right] \\ &= \frac{1}{2t}\left(\frac{g}{\langle B\rangle^2}-\frac{g}{B_N^2}\right).\end{aligned}$$

In our approximation we have assumed $t \ll 1$, and we have defined

$$\frac{1}{\langle B^2\rangle} = \frac{1}{B_N^2}+\sum\frac{\delta_{0,m}(\psi)}{B_N^2}\exp\left[-im\left(\frac{t\Phi_v}{g}+\beta\right)\right]$$

as the helical average of g/B^2. In the limit helical perturbations are weak, we also have $g = R_0B_0$, so that

$$\lambda = \frac{R_0B_0}{2t}\left(\frac{1}{\langle B\rangle^2}-\frac{1}{B_N^2}\right).$$

Thus, Eq. (6) becomes

$$d\Lambda_p^{(1)}/ds = (\partial p/\partial\psi)(B_0R_0/t)(1-B^2/B_N^2)/(B|\nabla\psi|^2)$$

where we ignore the helical contribution. The lowest order modulation, using $B \approx B_0(1-\varepsilon\cos\theta)$ and $|\nabla\psi_0| = B_0 r$, is

$$\Lambda^{(1)} = -\alpha\sin\theta$$

(see just after Eq. (4) for the definition of Λ). Thus we recover the tokamak shear modulation (see Eq. (10)). Now one notes that if $|\nabla\psi|^2$ is constant there is no pressure driven contribution to the average shear. To find a change of the average shear the correction to $|\nabla\psi|$ due to the toroidal shift of magnetic surface has to be taken into account. We use $\nabla\psi = \nabla(\psi_0+\psi_1)$, and that ψ_1 is related to the shift Δ by $\Delta\cos\theta = -\psi_1/|\nabla\psi_0|$. From Ref. 20 we have

$$\Delta = -r\varepsilon(4m-1)/[4m(m-1)]$$

and thus

$$\psi_1 = B_0R_0^2(4m-1)/[4m(m-1)]\varepsilon^3\cos\theta.$$

Then

$$|\nabla\psi|^2 = |\nabla(\psi_0+\psi_1)|^2 = |\nabla\psi_0|^2+2\nabla\psi_0\cdot\nabla\psi_1+\ldots = B_0^2r^2\{1+6\varepsilon\cos\theta(4m-1)/[4m(m-1)]\}$$

and the secular component of $\Lambda^{(1)}$ is

$$\Lambda^{(1)} = \alpha 3\varepsilon(4m-1)/[4m(m-1)]\theta \equiv \alpha S_1\theta. \tag{24}$$

The lowest order vacuum shear is readily calculated from Eq. (1) and using $\theta \approx \beta + t\varphi$. This yields

$$\Lambda^{(0)} = -(dt/d\psi)(|\nabla\psi|^2/B)\theta/t = -(d\ell nt/dr)(|\nabla\psi|/B)\theta \approx -(d\ell nt/d\ell nr)\theta.$$

The rotational transform can be expressed, near the axis, as[6]

$$t = \delta_m^2 m^4(m-1)n^{2m-3}/(m!^2 4m)(r/R_0)^{2m-4}.$$

Thus, we obtain

$$\Lambda^{(0)} = -2(m-2)\theta \equiv -S_0\theta$$

and the total integrated shear is

$$\Lambda = (-S_0 + S_1\alpha)\theta - \alpha\sin\theta. \tag{25}$$

This expression predicts the reversal of the shear at

$$\alpha_r = S_0/S_1 = 8m(m-1)(m-2)/[3\varepsilon(4m-1)]$$

which is verified in the numerical code for the Proto-Cleo example.

We now return to the ballooning equation for the tokamak and replace S by $-S_0+S_1\alpha$. We repeat the analysis and write the equation around a point of zero shear. We also need to take into account the helical modulation of the normal curvature, as the absolute value of the normal curvature is small near the zero shear point, which is near the vertical extremes of the flux surface. Thus we add to the toroidal normal curvature a term of the form

$$-R\kappa_n = a\cos p(\varphi-\varphi_0) \tag{26}$$

where $a$is the relative amplitude of the helical modulation (which we have extracted numerically from the actual fields), and p is the ratio of toroidal to helical curvature wavelengths along the field line, and is given by

$$p = (n/t) - m.$$

The phase φ_0 is included because along the field line the relative phase between the helical component and the toroidal shearless point is arbitrary, and we have to consider the worst case for instability.

The reduced ballooning equation for the stellarator is then written as

$$\begin{aligned} y'' &\approx -\alpha_e y \left\{ [F + a\cos\ p(\varphi - \varphi_0)]/\Lambda^2 - \alpha_e \varphi^2/\Lambda^4 \right\} && (27) \\ \Lambda &\approx |\Lambda_0| + \alpha_e \varphi/2 \\ F &= S/\alpha_e = (-S_0 + S_1\alpha_e)/\alpha_e \approx S_1 - S_0/\alpha. && (28) \end{aligned}$$

We solve Eq. (27) as we did in Eq. (15). We write $y = y_0 + y_1 + \ldots$ and we find the equations

$$\begin{aligned} y_0'' &= 0 && (29) \\ y_1'' &\approx -\alpha_e y_0 \left\{ [F + a\ \cos\ p(\varphi - \varphi_0)]/\Lambda^2 - \alpha_e \varphi^2/\Lambda^4 \right\}. && (30) \end{aligned}$$

As before, we take the solution y_0 =constant. Then,

$$\begin{aligned} \Delta y_1' &= -\alpha_e y_0 \int d\varphi \left[F/\Lambda^2 - \alpha_e \varphi^2/ + a\ \cos(p\varphi_0)\cos(p\varphi)/\Lambda^2 \right] \\ &= -y_0 \pi (\alpha_e/2)^{1/2} |\Lambda_0|^{-3/2} \left[F - (4|\Lambda_0|)^{-1} \right. \\ &+ \left. a\ \cos(p\varphi_0) \left(1 + p(2|\Lambda_0|/\alpha_e)^{1/2}\right) \exp\left(-p(2|\Lambda_0|/\alpha_e)^{1/2}\right) \right] \end{aligned}$$

and by demanding an intersection within one toroidal period we obtain the instability condition

$$y_0 + 2\pi \Delta y' < 0$$

which becomes

$$\min[G(|\Lambda_0|)] < 0 \qquad (31)$$

$$G(|\Lambda_0|) \equiv |\Lambda_0|^{3/2} \Big/ \left[(2\alpha_e)^{1/2}\pi^2\right] + (4|\Lambda_0|)^{-1} - F \tag{32}$$

$$-a\left[1 + p(2|\Lambda_0|/\alpha_e)^{1/2}\right] \exp\left[-p(2|\Lambda_0|/\alpha_e)^{1/2}\right] \tag{33}$$

where we have taken the worst phase condition, $\cos(p\varphi_0) = 1$.

Examination of the function G shows that at small α the minimum is positive, indicating the inherent low beta stability of stellarators. As α increases the minimum becomes negative, showing the existence of the ballooning instability. Analytically, we can see that at small the exponential term is very small; neglecting it we recover a tokamak-like criterion: $\min(G) = 0.3\alpha_e^{-1/5} - S/\alpha_e < 0$. More generally when the helical modulation is important we need to solve Eq. (28) numerically.

For the two flux surfaces of the Proto-Cleo that we have investigated we find:

- For $R = 0.435$ m, $S_0 = 2$, $S_1 = 0.13$, $p = 12.3$, $a = 0.7$, the analytic criterion predicts instability at $\alpha = 33$; the numerical code gives $\alpha = 16.7$.

- For $R = 0.425$ m, $S_0 = 2$, $S_0 = 0.094$, $p = 25.8$, $a = 0.5$, the analytic criterion predicts instability at $\alpha = 192$; the numerical codes gives $\alpha = 157$.

We can see that the analytic criterion gives a reasonable estimate of the instability threshold. The relatively bad prediction for the outer line can be partly understood if we consider the behavior of the ratio of the total curvatures. We have modeled the helical contribution in Eq. (26) as a sinusoidal function. However at the outer surface the higher harmonic terms of κ_n are important. Further, our analysis is strictly valid in the limit of large S and at the outer flux surface when $\alpha = 33$, $S = 2.3$, so that our analytic method can have a large error. For the inner flux surface where $\alpha = 192$, $S = 16$, and our method is clearly in the correct regime. Above the instability threshold the eigenfunction will narrow and isolate itself to a helical ripple. In that case the single point interaction analysis of Section IV applies. Instability will always be found as the normal curvature is biased to be destabilizing due to the positive average shear, which is roughly a factor of ε of the toroidal shear modulation, and from the helical contributions to the normal curvature, for

which one can find phases where the contribution is unfavorable. We note that if we allow for toroidal current it is possible to shift the zero shear points to the inside of the cross section, where the normal curvature is favorable.

VII Conclusions

We have examined the ballooning instability in toroidal systems, using a steep pressure gradient model. We can then evaluate the shear produced by the pressure driven Pfirsch-Schlüter currents. By focusing the investigation on the effect of the shearless points that arise when the pressure gradient is increased, we gain some insight in the second stability regime. In tokamaks it can be understood as a consequence of the shifting of these points away from the most unstable regions towards the top of the flux surface, where the destabilizing term is much weaker, and beyond a certain point it is insufficient to drive the instability. We have developed an analytic method that predicts the stability threshold and gives a second stability condition. Our results give a pessimistic outlook to the achieving of second stability since there is a very large unstable region before second stability sets in. However, we have only analyzed a circular cross-section, and considerable improvement in the threshold can be expected with shaping, if the point of zero geodesic curvature can be shifted inward to the region of favorable normal curvature.

In stellarators the case is more complicated. At low pressure gradients the point of zero shear occurs on the inner side of the flux surface, where the normal curvature is stabilizing. However, at large pressure gradients the Pfirsch-Schlüter currents can reverse the sign of the mean shear and one can find first ballooning instability. We further find that the helical modulation of the normal curvature is important in stellarators in establishing the threshold criterion.

We also note that as ballooning instability in stellarators with zero net toroidal current will always arise in the limit of arbitrarily large pressure gradients, it will probably be impossible to generalize the sharp boundary MHD equilibria studied in Ref. 16 to be a lowest order solution of a steep pressure profile MHD equilibria where $\partial p/\partial \psi$ is large. If a

stellarator has up-down symmetry, it may be shown that the marginally stable ballooning mode perturbation can also be made that retains this symmetry. The ballooning mode equation is essentially the same as the equilibrium equation for the line bending produced by the induced parallel currents as the pressure increases. Hence, the instability predicted in linear theory is an indication that ideal MHD equilibrium at a finite width with very large $\partial p/\partial \psi$ profile will not be found. However, it is still possible that the sharp boundary equilibria can be useful to describe sharp profile effects when some non-ideal features, as finite Larmor radius, are included, or if $\partial p/\partial \psi$ is considered bounded as has been treated in this paper.

Acknowledgments

We would like to acknowledge the computational help of Ting Ting Lee. The work was supported by the U.S. Department of Energy contract #DE-FG05-80ET-53088.

References

1. H.P. Furth, J. Killeen, M.N. Rosenbluth, and B. Coppi, in *Plasma Physics and Controlled Nuclear Fusion Research 1965*, (IAEA, Vienna 1966), vol. 1, p. 103.

2. B. Coppi, A. Ferreira, J.W.-K. Mark, and J.J. Ramos, Nucl. Fusion **19**, 715 (1979).

3. D. Lortz, and J.Nühremberg, Phys. Lett. **68A**, 49 (1978).

4. J.M. Greene, and M.S. Chance, Nucl. Fusion **21**, 453 (1981).

5. H.L. Berk, M.N. Rosenbluth, and J.L. Shohet, Phys. Fluids **26**, 2616 (1983).

6. V.D. Shafranov, Phys. Fluids **26**, 357 (1983).

7. M.S. Chance, R.L. Dewar, E.A. Frieman, A.H. Glasser, J.M. Greene, R. C. Grimm, S.C. Jardin, J.L. Johnson, J. Manickam, M. Okabayashi, and A.M. Todd, in *Plasma Physics and Controlled Nuclear Fusion Research* (Proc. 7th Int. Conf., Innsbruck, 1978), (IAEA, Vienna, 1979), vol. 1, p. 677; R.C. Grimm, R.L. Dewar, and J. Manickam, J. Comput. Phys. **49**, 194 (1983).

8. K.M. McGuire, Proc. Int. Conf. Plasma Physics, Proceedings Invited Papers, M.Q. Tran and R.J. Verbeek, Eds., Lausanne (1984) Vol. I, p. 123; C.K. Chu, A. Deniz, G.E. Georgiou, R.A. Gross, A.A. Grossman, A. Holland, R. Izzo, C. Kostek, F.M. Levinton, H.C. Lui, M. Machida, T.C. Marshall, R.L. Merlino, D. Oepts, G.A. Navratil, and P.G. Weber, Nucl. Fusion **25**, 1109 (1985).

9. M.N. Rosenbluth, S.T. Tsai, J.W. Van Dam, and M.G. Engquist, Phys. Rev. Lett. **51**, 1967 (1983).

10. A. Sykes, and M.F. Turner, in *Controlled Fusion and Plasma Physics* (Proc. 9th Europ. Conf., Oxford, 1979), (Culham Lab., Abingdon, U.K., 1979) EP22.

11. M.S. Chance, S.C. Jardin, and T.H. Stix, Phys. Rev. Lett. **51**, 1963 (1983).

12. J.M. Greene and J.L. Johnson, Plasma Phys. **10**, 729 (1968).

13. K.V. Roberts and J.B. Taylor, Phys. Fluids **8**, 315 (1965).

14. R.L. Dewar and A.H. Glasser, Phys. Fluids **26**, 3038 (1983).

15. J.P. Freidberg, Rev. Mod. Phys. **54**, 801 (1982).

16. H.L. Berk, J.P. Freidberg, X. Llobet, P.J. Morrison, and J.A. Tataronis, Phys. Fluids **29**, 3281 (1986).

17. W. Newcomb, Ann. Phys. **10**, 232 (1960).

18. Liu Chen and M.S. Chance, Bull. Am. Phys. Soc. **31** 9, 1603 (1986).

19. A.H. Boozer, Phys. Fluids **24**, 1999 (1981).

20. A.I. Morozov, and L.S. Solov'ev, in *Reviews of Plasma Physics*, (Consultants Bureau, New York, 1965), vol. 2, p. 1.

Characteristic		
Major radius	$R_0(m)$	0.400
Minor radius	$a(m)$	0.093
Number of field periods	n	7
Winding multipolarity	m	3
Winding law		$\phi = (m/n)\theta$
Number of helices		2
θ_{helix} and $\phi = 0$		0
		60°
Helical currents	(MA)	± 0.020
Toroidal field current	(MA)	0.600

Table I. Parameters determining magnetic fields in Proto-Cleo. Coils are wound around a surface of revolution generated by rotating a circle of radius a whose center is a distance R_0 from the axis. The toroidal angle is ϕ and the poloidal angle is θ.

Figure Captions

Figure 1. The solid curve shows the critical value of the parameter F in the single interaction model, $F_c(\Lambda_0)$. The dashed line is the variational upper bound $F_c^v(\Lambda_0)$, and the dotted line is the limit $-1/(4\Lambda_0)$ of $F_c(\Lambda_0)$ at large negative values of Λ_0.

Figure 2. Ballooning instability domain in the A-plane, at $S = 10.0$.

Figure 3. Second stability boundary as a function $\log\alpha$ vs. $\log\ S$. The dots denote the numerical solution, and the solid straight line is a linear fit at large values of S. The dashed line is the prediction at low S given in Ref. 3. The crosses represent the criterion obtained in this paper.

Figure 4. Several computed quantities of Eq. (16). Panel (a) shows the integrated shear function Λ for a case very close to second stability: $S = 10.0$, $\alpha = 60.93$, $A = 15.10$. In panel (b) the function $1/f$ is plotted. Panel (c) shows the graphs of the solution y of the Schrödinger equation (Eq. (4)) for two different values of the parameter A: the top graph is for $A = 15.11$ (stable), the bottom graph is for $A = 15.09$ (unstable).

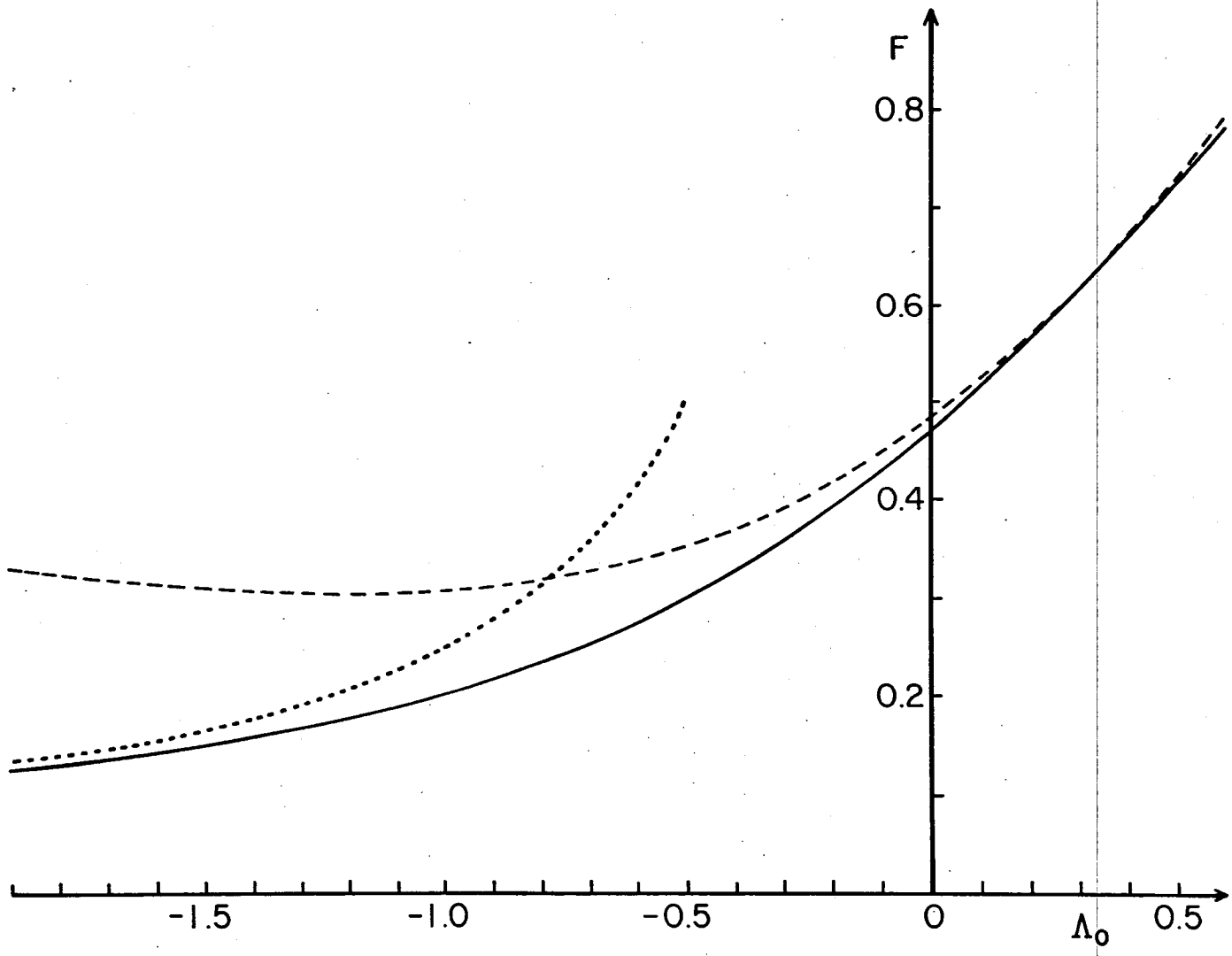

Fig. 1

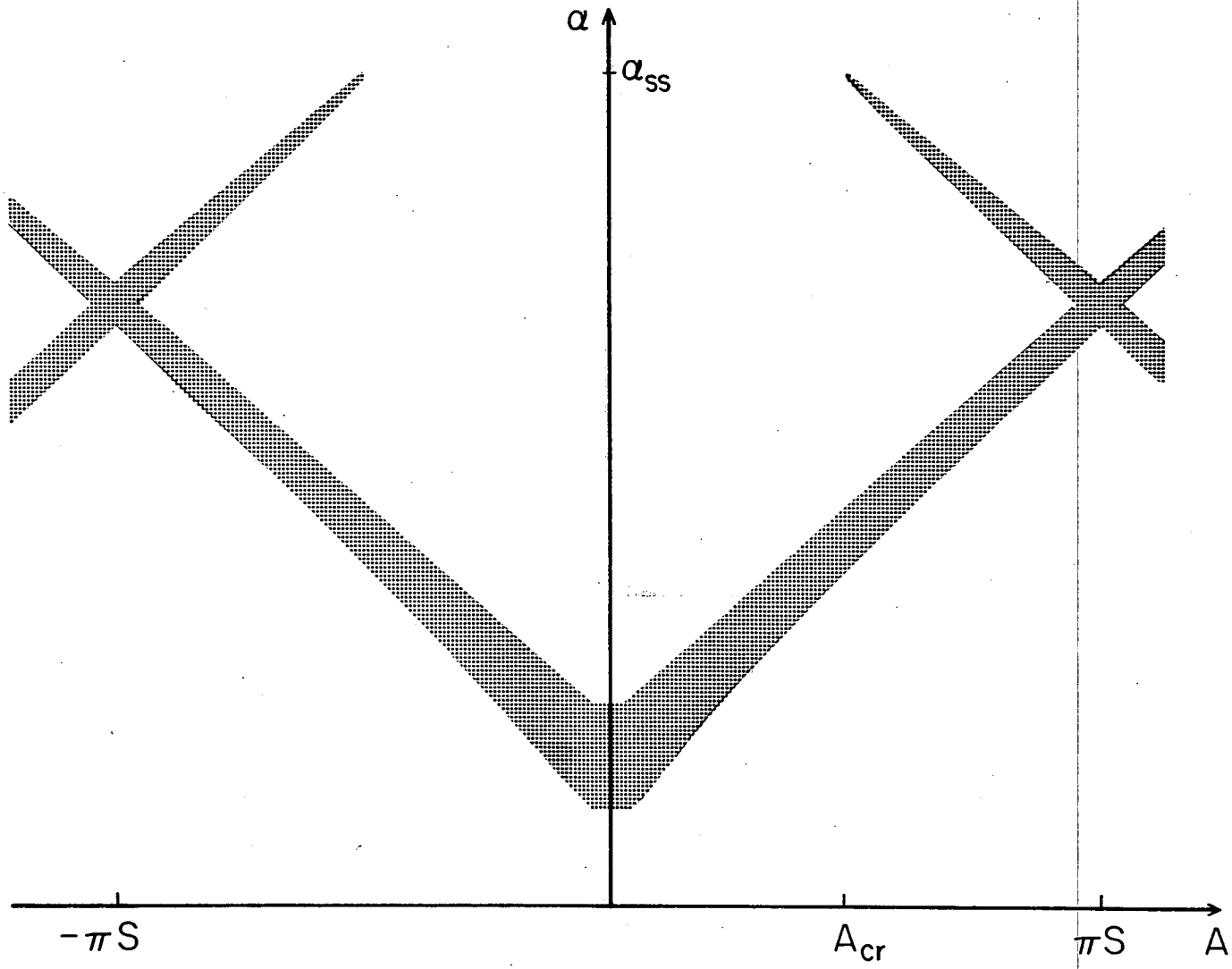

Fig. 2

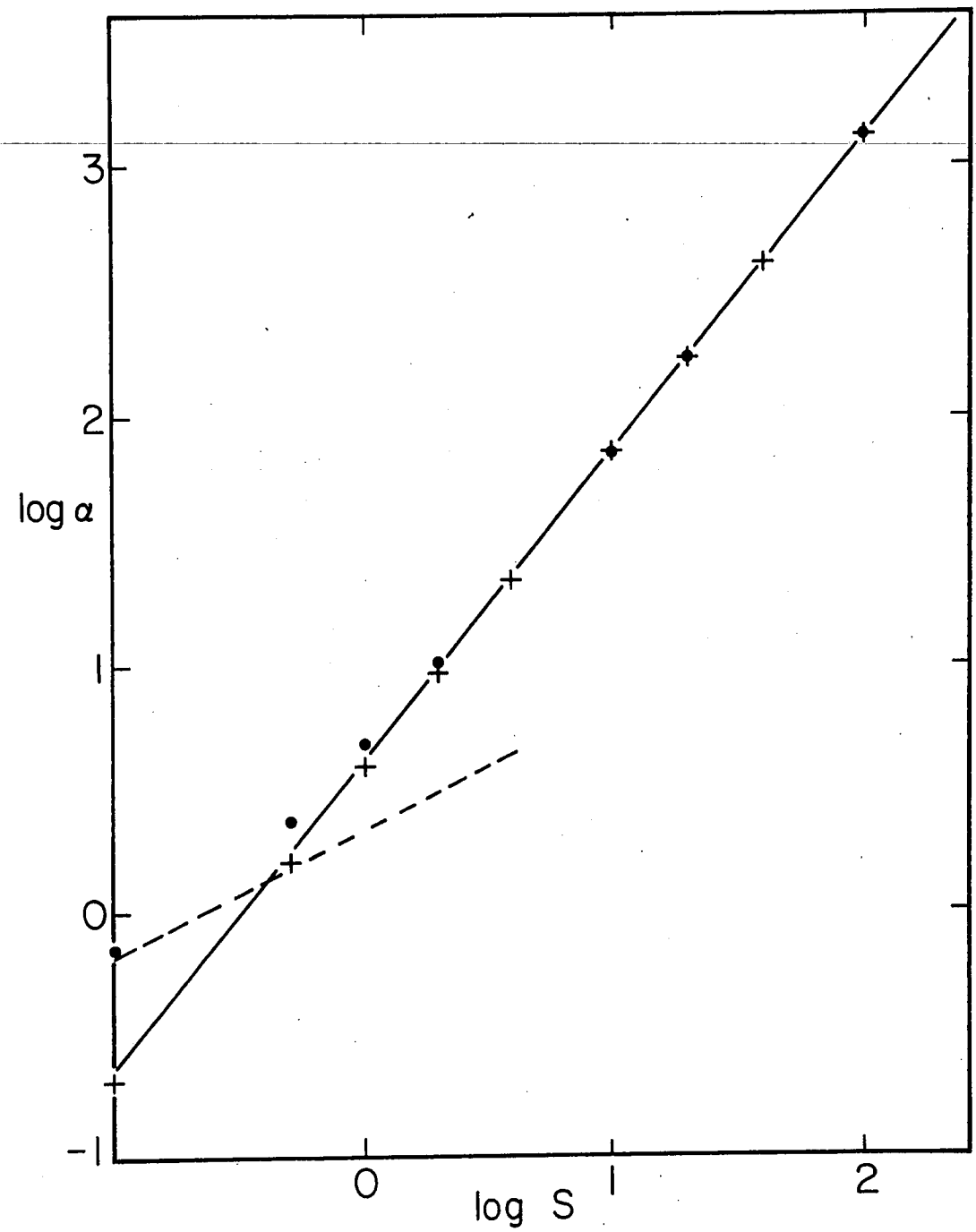

Fig. 3

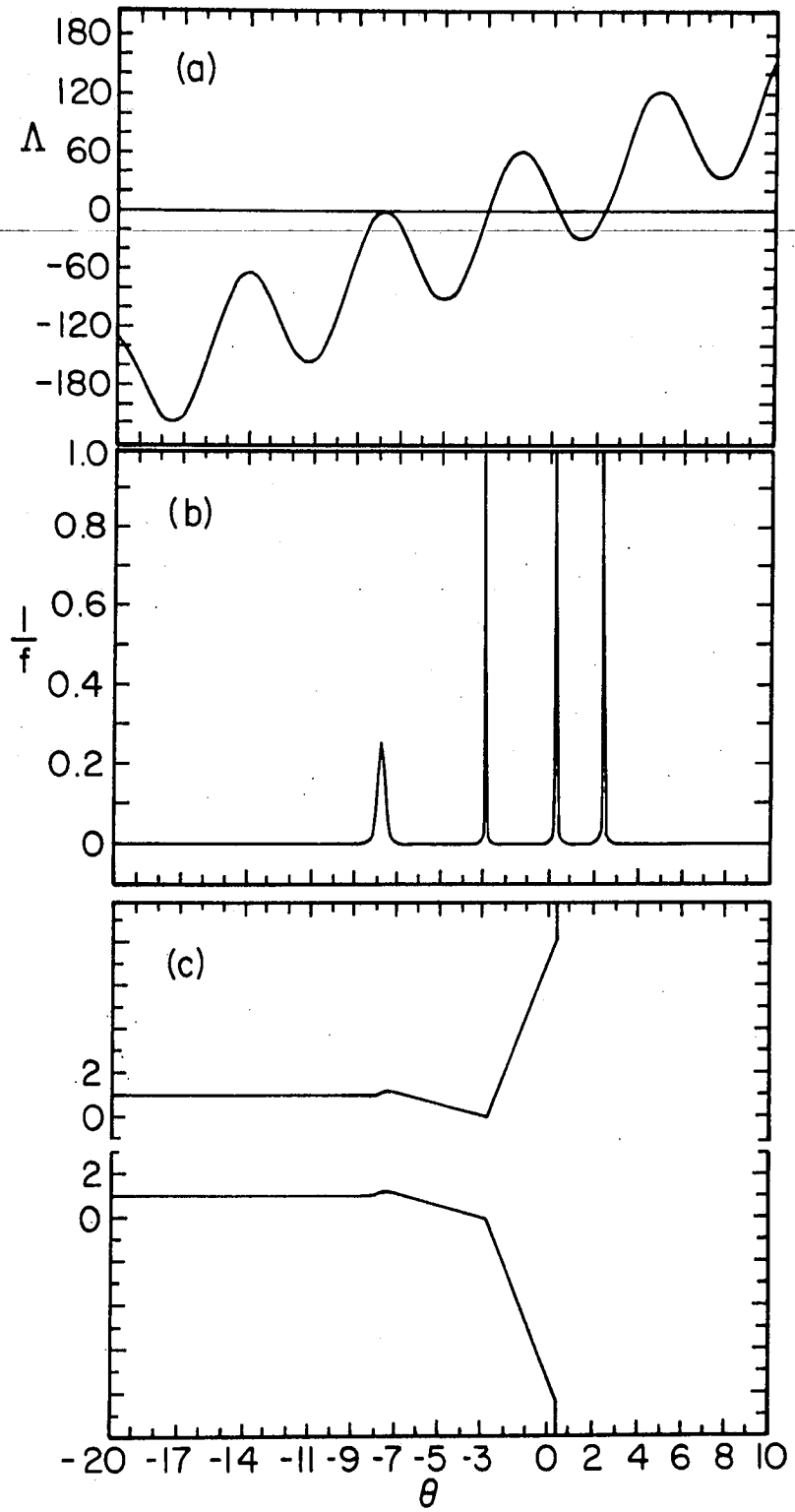
(a)
Λ
180
120
60
0
-60
-120
-180
(b)
1/f
1.0
0.8
0.6
0.4
0.2
0
(c)
2
0
2
0
-20 -17 -14 -11 -9 -7 -5 -3 0 2 4 6 8 10
θ

Fig. 4